# Thermal-hydraulic and Neutronic Design
# for a Super Critical Water Reactor
# using Nanofluid as Coolant

*Takhshid, Homa; Jahanfarnia, Gholamreza [*][+]; Kheradmand Saadi, Mohsen; Rahimi, Mohammad Hossein*

*Department of Nuclear Engineering, Science and Research Branch, Islamic Azad University, Tehran, Iran*

**ABSTRACT**

*The most important intrinsic limitation of conventional coolant fluids is their relatively low thermal conductivity. In this regard, in the last two decades, by introducing a new concept called nanofluid, researchers have improved the thermal conductivity of conventional coolants; furthermore, thermal efficiency as well as convection heat transfer of the thermal-hydraulic cycles is increased by applying coolants at supercritical pressures. A supercritical water reactor is one of the generation IV reactors, which is basically a creative mixture of conventional pressurized water reactors and supercritical pressure steam boilers. In the present study, by applying the concept of nanofluid coolants in a typical supercritical pressure water reactor, thermo-neutronic behavior of the reactor core was investigated. In this manner, thermodynamic properties of the applied coolant were evaluated by adding numerical models of nanofluid properties to the IAPWS-IF97, and for simulation of the thermal-hydraulic behavior of the coolant, a modular computer code has been developed using the C# programming language based on the porous media approach, and neutronic simulation was performed by the MCNP code. Final results showed that application of a water-based $Al_2O_3$ nanofluid with ~11% mass fraction (~2% volume fraction at core inlet) as coolant without any violation of neutronic characteristics of the core is achievable and the criticality of the core would be sustained. Calculations indicate that applying nanofluids to the core will flatten the radial neutron flux in the reactor core, and the convection heat transfer coefficient will improve by 2%.*

**KEYWORDS:** *Supercritical Water Reactors; Thermal-hydraulic and Neutronic Analysis; Nanofluid; MCNP code; C# programming language.*

[*]To whom correspondence should be addressed.
[+]E-mail address: jahanfarnia@srbiau.ac.ir
Tel.: +989126542844; fax: +98 21 44817170

## INTRODUCTION

A brief review of coal-fired power plants in the last 50 years; Fig. 1 illustrates a remarkable increase in the net efficiency of the plant from 37% in the 1970s to more than 46% in 2015. By introducing a new set of steel alloys in the boiler manufacturing industry in 1990, this enhancement was characterized by an increase in live steam temperature beyond 550°C, when boiler steels became available, which allowed them to exceed the former material limits. Along with the temperature increase, the steam pressure was shifted up to the supercritical pressure region (>221 [bar]) to maximize the turbine power. Meanwhile, In comparison with such development, the net efficiency of the latest pressurized water reactors (PWR), which is around 36%, is still close to the efficiency of the first generation of light water reactors (which were 34%) [1].
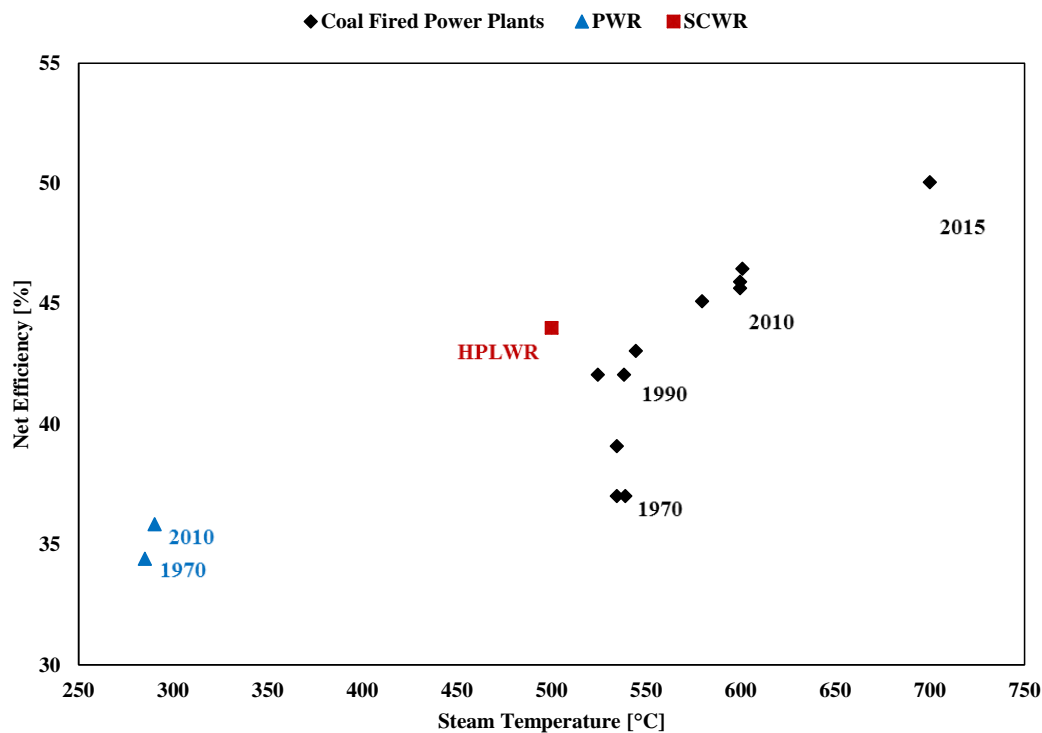


*Fig. 1: Increase of the net efficiency with live steam temperature of different thermal power plants [1]*

This comparison had motivated the Generation IV International Forum to look for similar options for future light water reactors with superheated steam at supercritical pressure, called Supercritical Water-Cooled Reactors (SCWR) [1].

The early concept of a direct-cycle supercritical-pressure light water reactor was proposed and developed over the 1990s. A SCWR has an inlet coolant density of approximately 800 kg/m3 and an outlet coolant density of around 100 kg/m3 Therefore, The enormous variation in coolant density introduces challenges, such as changing the core slowing-down cross-section field, and has a significant impact on power distribution, so coupling neutronic calculations with thermal-hydraulic mathematical computations is crucial for SCWR [2–4]. Attempts to achieve an optimal fuel assembly and core design led to an efficient design known as the European High Performance Light Water Reactor (HPLWR) with Boiling Water Reactor (BWR)-type fuel assemblies [5–9], see Fig. 2. D.

Bittermann, et al. proposed the steam cycle (Fig. 3) for a high-performance light water reactor [10], which was later optimized by Brandauer et al. for steady-state, full load conditions using the thermodynamic code IPSE-Pro 4.0 see Fig. 4 [11].
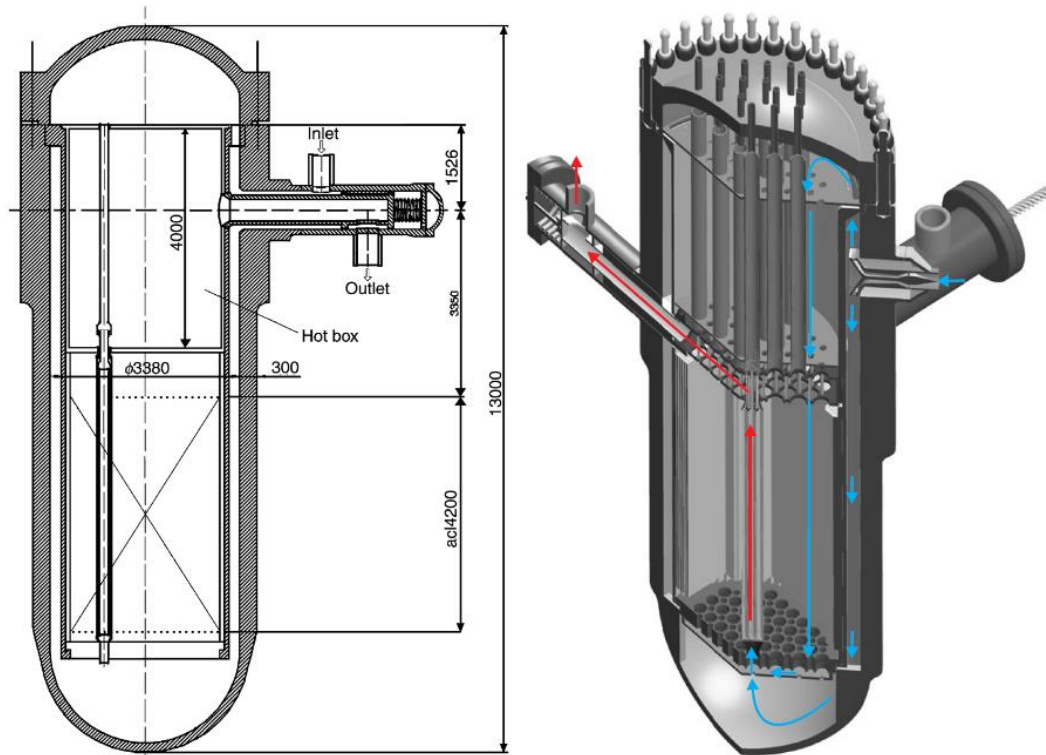


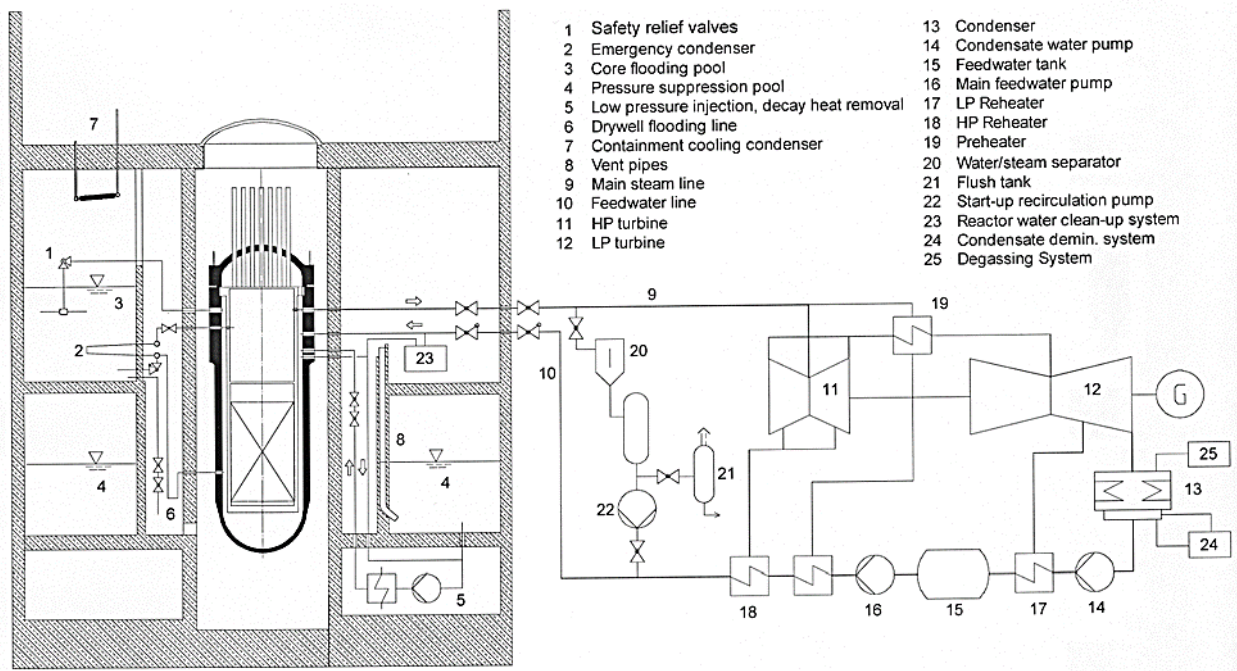*Fig. 2: Single-pass core design with indicated flow path [12]*



| 1 | Safety relief valves | 13 | Condenser |
|---|---|---|---|
| 2 | Emergency condenser | 14 | Condensate water pump |
| 3 | Core flooding pool | 15 | Feedwater tank |
| 4 | Pressure suppression pool | 16 | Main feedwater pump |
| 5 | Low pressure injection, decay heat removal | 17 | LP Reheater |
| 6 | Drywell flooding line | 18 | HP Reheater |
| 7 | Containment cooling condenser | 19 | Preheater |
| 8 | Vent pipes | 20 | Water/steam separator |
| 9 | Main steam line | 21 | Flush tank |
| 10 | Feedwater line | 22 | Start-up recirculation pump |
| 11 | HP turbine | 23 | Reactor water clean-up system |
| 12 | LP turbine | 24 | Condensate demin. system |
| | | 25 | Degassing System |

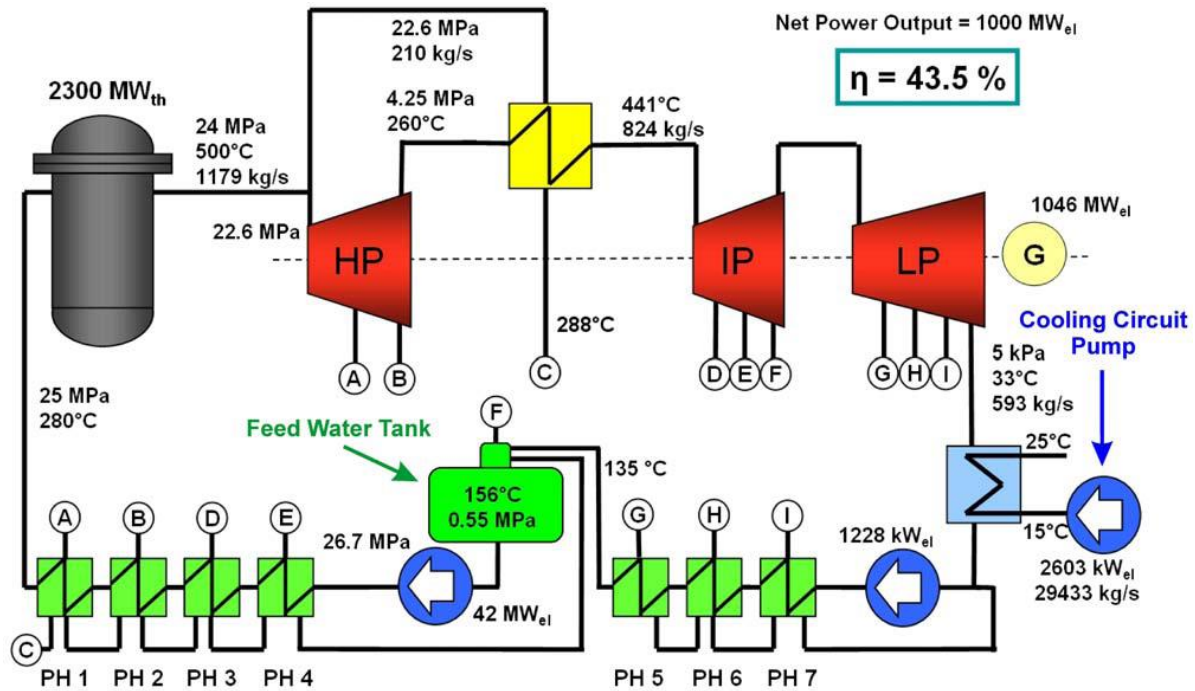*Fig. 3: Sketch of the HPLWR safety systems and steam cycle [10]*

*Fig. 4: Modified schematic diagram of the HPLWR steam cycle [11]*

As one may know, among the in-core structure components of a typical SCWR, the fuel cladding faces the most severe working conditions (working temperature up to 600 °C) [13]. Buongiorno and Hu [14] carried out a project in a nuclear reactor to investigate the CHF of nanofluids and mechanisms of enhanced heat transfer. The authors reported that the project findings were significant and new and could impose a significant improvement in both economic performance and safety margins. Thermal-hydraulic analysis of the Canadian SCWR was conducted to account for variations in thermo-physical parameters of Al2O3 nanoparticles with different mass fractions (from 0.1 to 40%). The comes about appear that when using alumina nanofluid with a mass fraction of 40% nanoparticles, the maximum temperatures of the clad and fuel decrease by about 20 °C and 30 °C, respectively [15]. Among the many advantages of nanofluids over conventional solid-liquid suspensions, the following are worth mentioning [16, 17]: higher specific surface area, higher stability of the colloidal suspension, lower pumping power required to achieve the equivalent heat transfer, reduced particle clogging compared to conventional colloids, and higher level of control of the thermodynamics and transport properties by varying the particle material, concentration, size, and shape.

Several authors have investigated different aspects of applying water-based nanofluids in pressurized water reactors as coolants; thermal-hydraulic analysis of applying such coolants was performed by Zarifi, et al. [18] in 2013, but as one knows, the introduction of any new material in a nuclear core will induce a neutronic feedback on fission power production; therefore in general, a coupled thermal–hydraulic and neutronic study for the utilizing of nanofluids in light water reactors is inevitable. Safarzadeh and Nourollahi [19, 20] have investigated the coupled neutronic/thermo-hydraulic analysis of water/ $Al_2O_3$ nanofluids in a VVER-1000 reactor with different methods.

According to the study [21], thermal-hydraulic analysis of applying a water-based Al2O3 nanofluid with different nanoparticle mass fractions was investigated using a porous media approach. The advantages of using nanofluids

include better heat transfer characteristics and improved thermal conductivity compared to base fluids, so the heat transfer capacity in the reactor core will be higher. Calculations showed that the utilization of nanofluid can enhance the convection heat transfer coefficient of coolant and the fuel cladding temperature, as well; meanwhile, as we mentioned, a coupled neutronic/thermo-hydraulic analysis is needed for an accurate assessment of applying $Al_2O_3$ nanofluid in a typical SCWR core.

In this study for a coupled thermo-neutronic calculation, a modular computer code has been developed using a C# programming language based on a porous media approach to simulate the thermal-hydraulic behavior of the coolant, and neutronic simulation was performed by MCNP code. Previous studies focused on thermal-hydraulic analysis and used power distribution as an existing reference without calculations or couplings. For the purpose of illustration and comparing the final results, the subsequent calculations are performed for the single-pass core design of those selected by C. Waata [22], see Fig. 5; the main characteristics of the selected reactor core and the operating conditions (pressure, mass flow rate and coolant inlet temperature) are presented in Table 1. Another important element in this article is that nanofluids can improve heat transfer efficiency in SCWRs, which are attractive due to their economic viability. The main objective of these coupled calculations is to evaluate the possibility of using water-based Al2O3 nanofluid as a coolant in a typical SCWR, to what extent the nanoparticle concentration can be increased, and whether the reactor remains in a critical state and achieves a uniform power distribution.

Table 1: Main characteristics of the single-pass core design [22]

| Parameter | Value |
|---|---|
| *Core* | |
| *Thermal power* | *2075 [MW]* |
| *Inlet Temperature* | *280 [°C]* |
| *Outlet pressure* | *250 [bar]* |
| *Inlet mass flow rate* | *1060 [kg/s]* |
| *Relative mass flow rate through downcomer* | *75.0 [%]* |
| *Relative mass flow rate through the moderator box* | *8.32 [%]* |
| *Relative mass flow rate through the assembly gap* | *16.65 [%]* |
| *Fuel Assembly* | |
| *Active length* | *4200 [mm]* |
| *Fuel rod diameter* | *8.00 [mm]* |
| *Cladding thickness* | *0.50 [mm]* |
| *Gap between cladding and fuel pellet* | *0.15 [mm]* |
| *Pitch/Diameter ratio* | *1.15* |
| *Moderator box length* | *26.00 [mm]* |
| *½ gap around one fuel assembly* | *5.00 [mm]* |
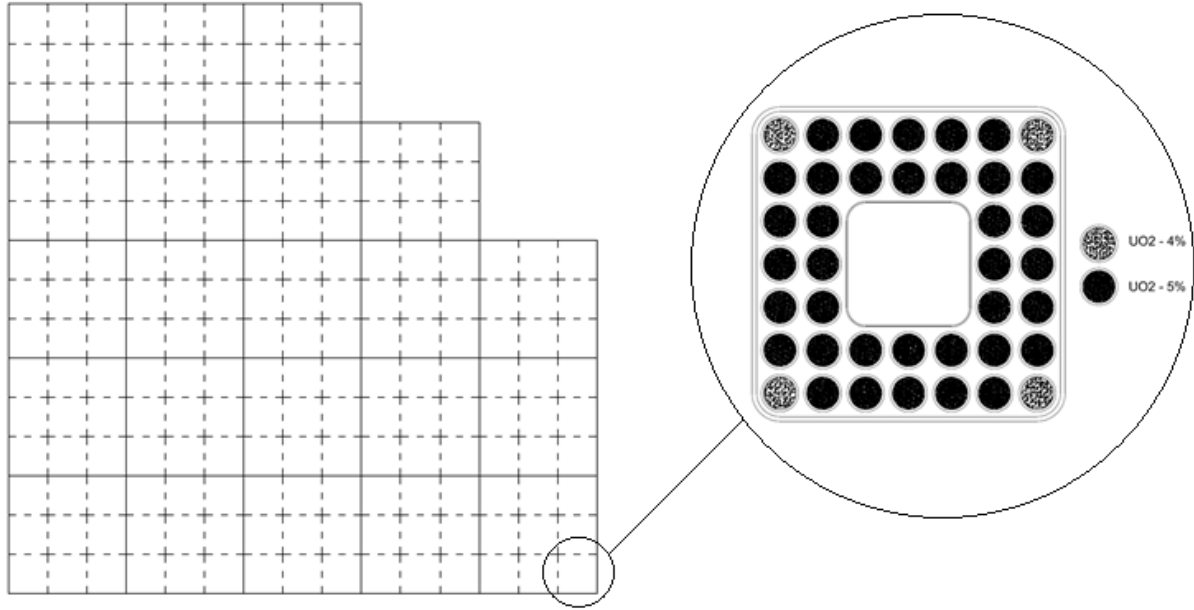
*Fig. 5: Fuel assembly and core configuration in the single-pass core design [22]*

## MATERIAL AND METHODS

### Thermodynamic properties of water-based Al₂O₃ nanofluid

Consider a homogeneous colloid made of a base fluid and nanoparticles, called nanofluid, in an arbitrary control volume, $_V$ (see Fig. 6). Regarding this definition, the nanoparticles *Mass Fraction* and *Volume Fraction* can, respectively, be described as [21]:

$$\varphi_M = \frac{M_{\text{Nanopartide}}}{M_{NanoFluid}}$$

(Eq. 1)

$$\varphi_V = \frac{V_{\text{Nanopartide}}}{V_{NanoFluid}} = \frac{\rho_{\text{BaseFluid}}}{\rho_{\text{BaseFluid}} + \rho_{\text{Nanopartide}} \cdot \frac{(1-\varphi_M)}{\varphi_M}}$$

(Eq. 2)
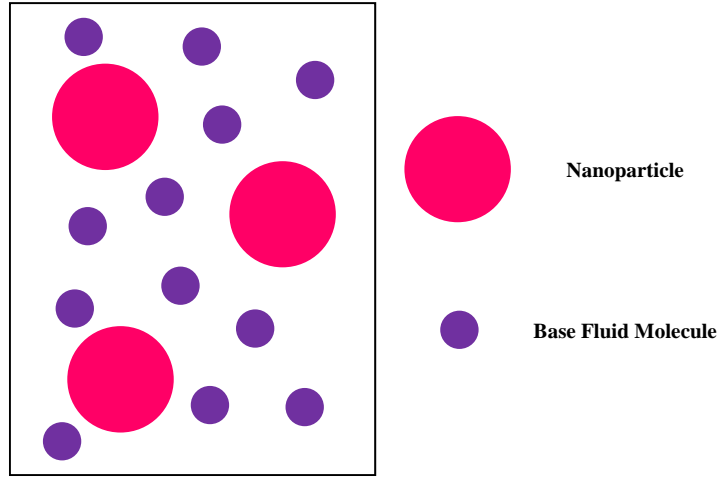
*Fig. 6: Homogeneous Nanofluid in an arbitrary control volume [21]*

Based on these definitions, the altered intrinsic properties of the base fluid (Al$_2$O$_3$ nanofluid), Density ($\rho$), Specific Isobaric Heat capacity ($C_P$), Viscosity ($\mu$) and Thermal Conductivity ($K_e$), can be calculated using the following relations, respectively [21]:

$$\rho_{NanoFluid} = \varphi_V \cdot \rho_{\text{Nanopartide}} + (1 - \varphi_V) \cdot \rho_{\text{BaseFluid}} \tag{Eq. 3}$$

$$C_{P-NanoFluid} = \frac{\varphi_V \cdot (\rho.C_P)_{\text{Nanopartide}} + (1 - \varphi_V) \cdot (\rho.C_P)_{\text{BaseFluid}}}{\varphi_V \cdot \rho_{\text{Nanopartide}} + (1 - \varphi_V) \cdot \rho_{\text{BaseFluid}}} \tag{Eq. 4}$$

$$\mu_{NanoFluid} = \mu_{\text{BaseFluid}}\left(1 + 7.3\varphi_V + 123\varphi_V^2\right) \tag{Eq. 5}$$

$$k_{e-NanoFluid} = k_{\text{e-BaseFluid}}\left(1 + 2.72\varphi_V + 4.97\varphi_V^2\right) \tag{Eq. 6}$$

*Thermal-hydraulic Approach*

Fig. 7 shows an arbitrary field in which includes a single-phase fluid and distributed solids, in which heat may be generated or absorbed by the solid structure. For an arbitrary point in the domain, we associate a closed surface $A_T$ as enclosing a volume, $V_T$. The portion of $V_T$ which contains the fluid is $V_f$. The total fluid-solid interface within the volume $V_T$ is $A_{fs}$. The portion of $A_T$ through which the fluid may flow is $A_f$. The ratio of the fluid volume $V_f$ to the total volume $V_T$ is defined as the volume porosity, i.e. $\gamma_V = \dfrac{V_f}{V_T}$.
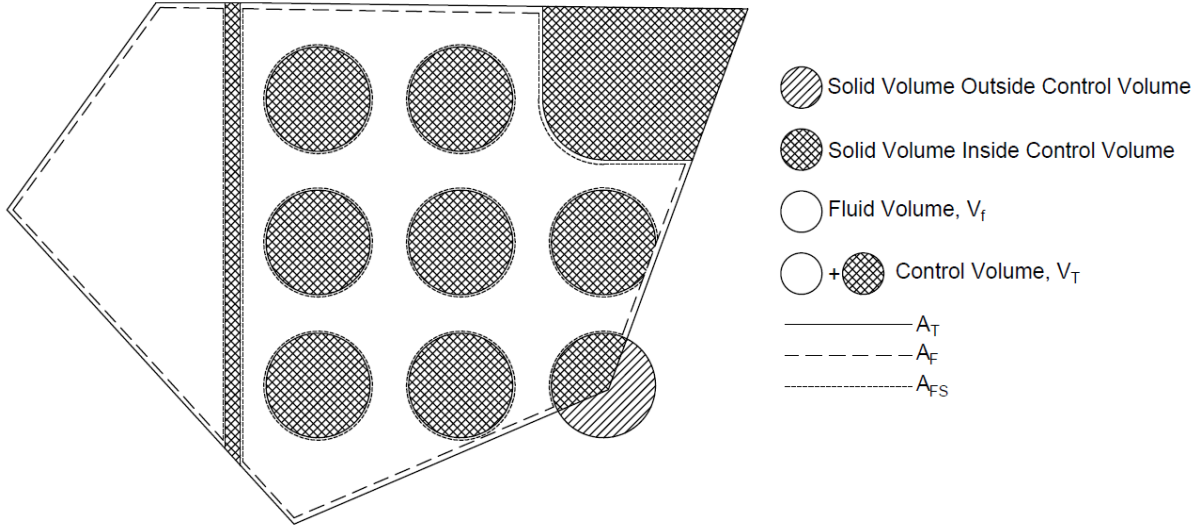
*Fig. 7: Region consisting of a single-phase fluid with stationary solids [23]*

The porous media approach states the steady-state conservation equations of mass, momentum and energy in an arbitrary Cartesian coordinate system as follows [23, 24]:

$$\frac{\Delta_x\left(\gamma_{Ax}^{\;i(x)}\left\{\rho v_x\right\}\right)}{\Delta x} + \frac{\Delta_y\left(\gamma_{Ay}^{\;i(y)}\left\{\rho v_y\right\}\right)}{\Delta y} + \frac{\Delta_z\left(\gamma_{Az}^{\;i(z)}\left\{\rho v_z\right\}\right)}{\Delta z} = 0 \tag{Eq. 7}$$

$$\frac{\Delta_x\left(\gamma_{Ax}^{\;i(x)}\left\{\rho v_z v_x\right\}\right)}{\Delta x} + \frac{\Delta_y\left(\gamma_{Ay}^{\;i(y)}\left\{\rho v_z v_y\right\}\right)}{\Delta y} + \frac{\Delta_z\left(\gamma_{Az}^{\;i(z)}\left\{\rho v_z v_z\right\}\right)}{\Delta z} = -\frac{\Delta_z\left(\gamma_{Az}^{\;i(z)}\left\{P\right\}\right)}{\Delta z}$$

$$-\gamma_V^{\;i}\langle\rho\rangle g_z + \frac{\Delta_x\left(\gamma_{Ax}^{\;i(x)}\left\{\tau_{xz}\right\}\right)}{\Delta x} + \frac{\Delta_y\left(\gamma_{Ay}^{\;i(y)}\left\{\tau_{yz}\right\}\right)}{\Delta y} + \frac{\Delta_z\left(\gamma_{Az}^{\;i(z)}\left\{\tau_{zz}\right\}\right)}{\Delta z} + \gamma_V^{\;i}\langle R_z\rangle \tag{Eq. 8}$$

$$+\frac{\Delta_x\left(\gamma_{Ax}^{\;i(x)}\left\{\rho U v_x\right\}\right)}{\Delta x} + \frac{\Delta_y\left(\gamma_{Ay}^{\;i(y)}\left\{\rho U v_y\right\}\right)}{\Delta y} + \frac{\Delta_z\left(\gamma_{Az}^{\;i(z)}\left\{\rho U v_z\right\}\right)}{\Delta z} = -\gamma_V^{\;i}\left\langle\rho\left(\frac{\partial v_x}{\partial x} + \frac{\partial v_y}{\partial y} + \frac{\partial v_z}{\partial z}\right)\right\rangle$$

$$+\frac{\Delta_x\left(\gamma_{Ax}^{\;i(x)}\left\{k_e\frac{\partial T}{\partial x}\right\}\right)}{\Delta x} + \frac{\Delta_y\left(\gamma_{Ay}^{\;i(y)}\left\{k_e\frac{\partial T}{\partial y}\right\}\right)}{\Delta y} + \frac{\Delta_z\left(\gamma_{Az}^{\;i(z)}\left\{k_e\frac{\partial T}{\partial y}\right\}\right)}{\Delta z} + \gamma_V\left(^{i}\langle q_{rb}'''\rangle + ^{i}\langle q'''\rangle + ^{i}\langle\phi\rangle\right) \tag{Eq. 9}$$

The calculation flow chart is illustrated in Fig. 8; detailed descriptions of the above-mentioned equations are well discussed in our early reports [23, 24]. The main idea of this study is to evaluate the coupled thermo-neutronic calculation of applying a water based nanofluid in a SCWR. A set of six different mass fractions have been considered (Applying nanofluid coolant section). Thermal- hydraulic boundary conditions are listed in Table 2.

Table 2: Thermo-hydraulic boundary conditions of the simulation

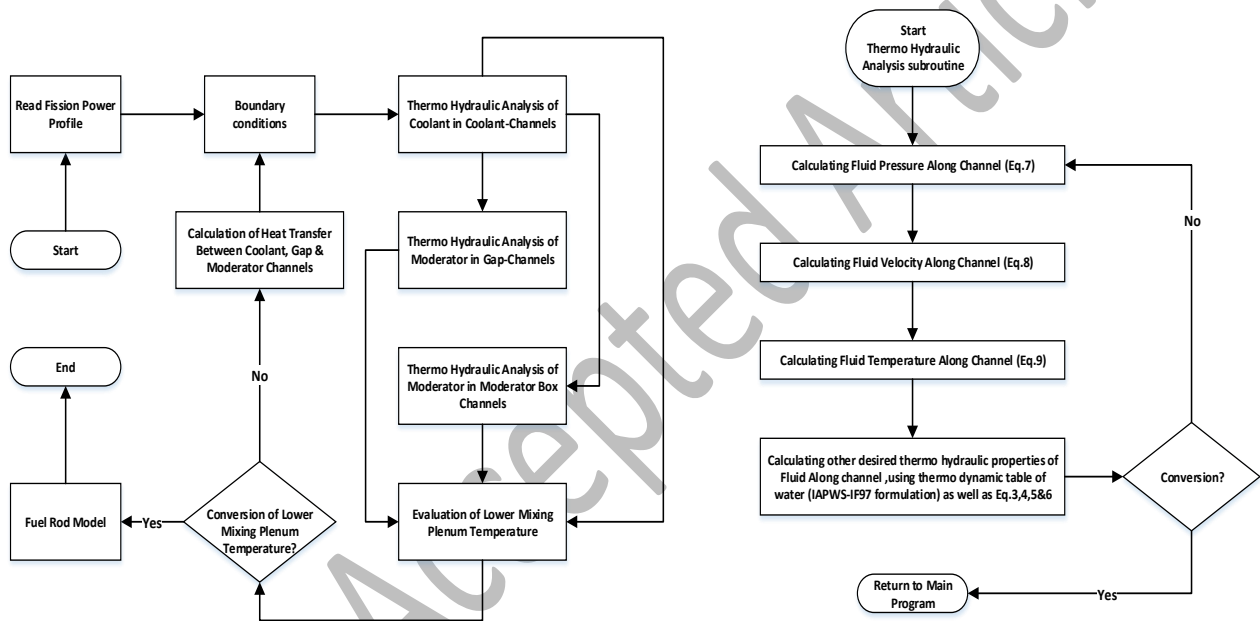| Boundary Condition | Value |
|---|---|
| Lower Mixing Plenum Temperature | 305.1 C |
| Average Coolant Inlet Velocity in Evaporator | 1.217 m/s |
| Core Outlet Pressure | 250 [bar] |
| Thermal Core Power | 2075 [MW] |



*Fig. 8: Flow chart of thermal- hydraulic calculation*

### Fuel rod model

By applying the porous media approach for coolant simulation, the fuel rod modeling can be performed independently, i.e., the evaluated temperature for the coolant medium of each axial mesh is applied as the surface boundary condition of the fuel rod; Later on, by using Newton's law of cooling, Poisson's equation (steady-state heat transfer) and MATPRO library [25] (Fig. 9), as well as Calza-Bini's method [27] fuel rod temperature profile can be obtained; see Fig. 10.
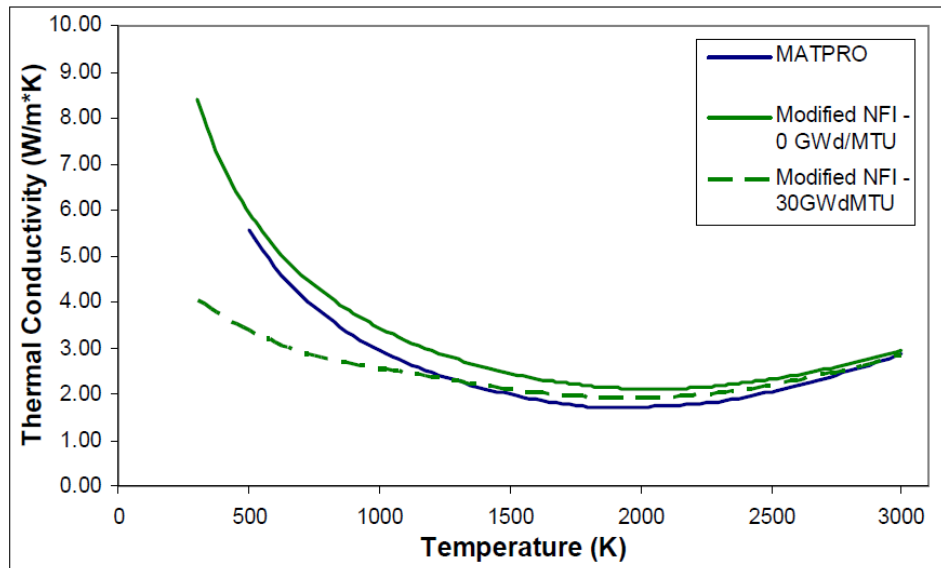
**Fig. 9: MATPRO and modified NFI thermal conductivity models for UO2 as a function of temperature [26]**
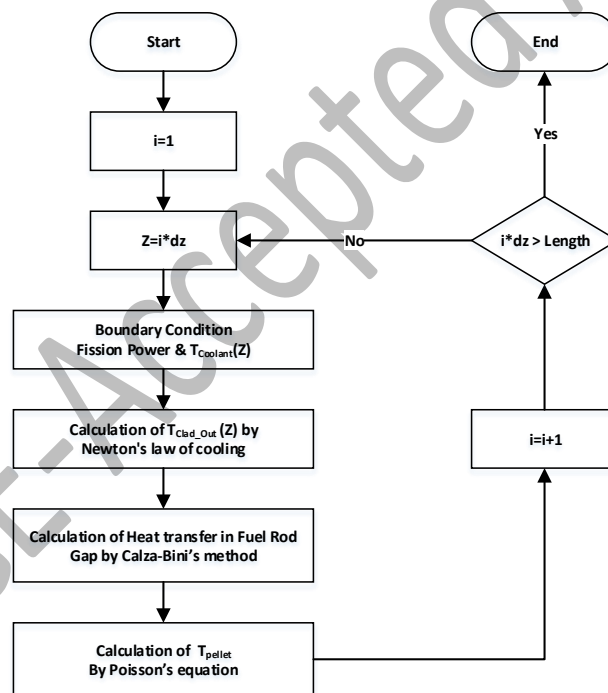


**Fig. 10: Fuel rod modeling flow chart**

*Neutronic calculations*

An MCNP 3-dimensional model can be widely used to evaluate various parameters, such as power distribution. According to the properties of materials and components, 21 meshes (universes) with different properties are considered in the fuel assemblies in order to perform accurate calculations (single-path design). An axial (A) and radial (B) cross-sectional view of the reactor core is shown in Fig. 11.
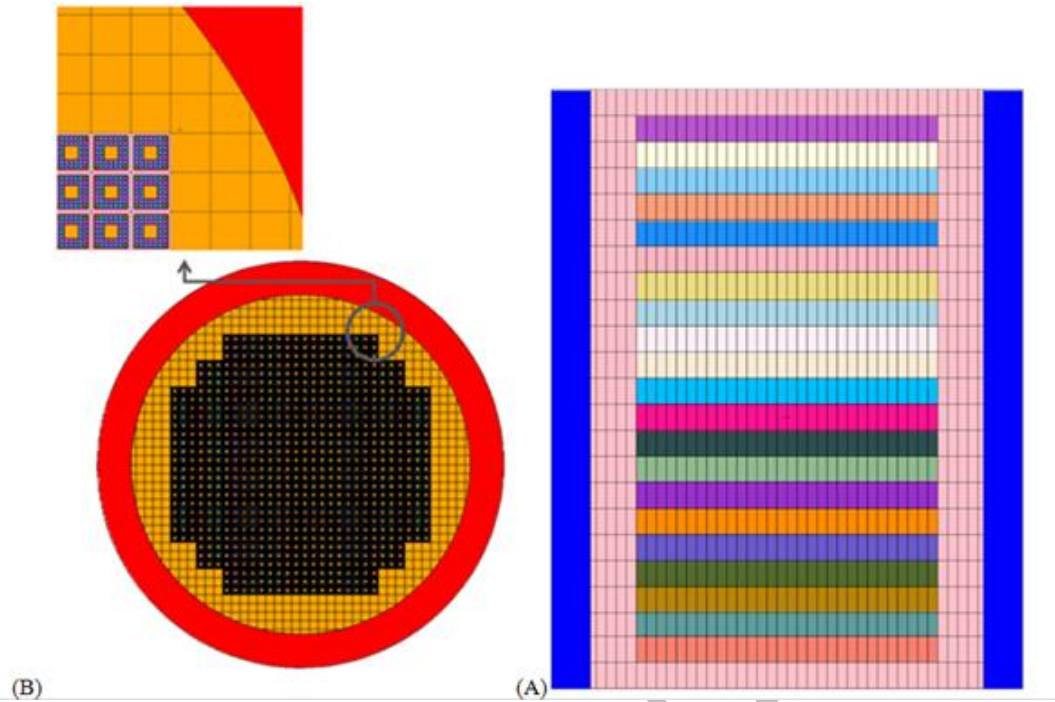
*Fig. 11: Axial (A) and radial (B) cross-sectional view of the single-path reactor*

The Monte Carlo MCNP code is used to simulate the neutrons and their average behavior in the reactor core with a modified multi-temperature ENDFVII based library [28]. The library contains cross-section data at four temperatures for all materials (293.6 K, 600 K, 900 K and 1200 K) in order to appropriately keep in count the Doppler Effect. As Conti reported [29], in order to realistically sample the neutrons' lethargy step by a collision, a ruse was applied to effectively represent and update each fuel zone's composition: in the material card corresponding to a certain fuel zone, each nuclide's atomic fraction is split up into two components, referring to the available libraries having temperatures closest (higher and lower) to the fuel zone's. The total atomic fraction is partitioned among the two components according to the proximity of their temperature to the fuel zone's, as schematized in Fig. 12. By utilizing MCNP, it is possible to determine the amount of heating energy deposition from the fission process and predict the power profiles of individual fuel rods. The same geometry model in thermal-hydraulic calculations is used for neutronic analysis. The input card for MCNP simulation describes the physical model: the geometry, materials, cross-section data library, and type of output required. Table 3 shows the physical constraints in MCNP

Table 3: Boundary conditions in MCNP

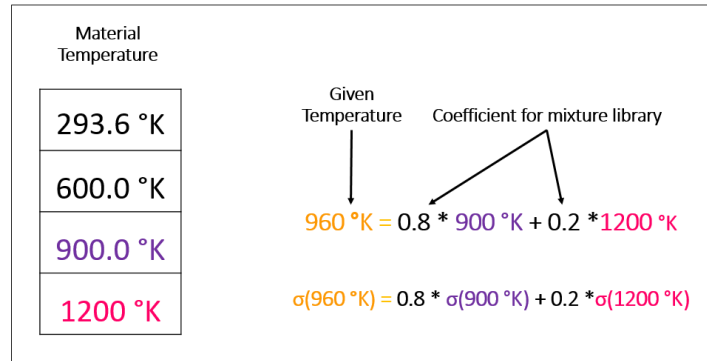| Parameters MCNP input Density | Density [kg/m³] | Temperature of the cross-section library (°C) |
|---|---|---|
| Fuel - UO2 (5% enrichment and 4% in the corner rod) | 10600 | 1227 |
| Cladding - Alloy 316 | 7450 | 527 |
| Moderator | 769 | 287 |
| Coolant | 769 | 287 |

*Fig. 12: Calculation method for the Doppler Effect in fuel material [29]*

### Coupling process

As mentioned earlier, the introduction of any new material in a nuclear core will induce a neutronic feedback on fission power production, which needs to be carried out in a coupled thermo-neutronic calculation. The adopted calculation flow chart for compensation of neutronic feedbacks in thermal-hydraulic analysis is depicted in Fig. 13.
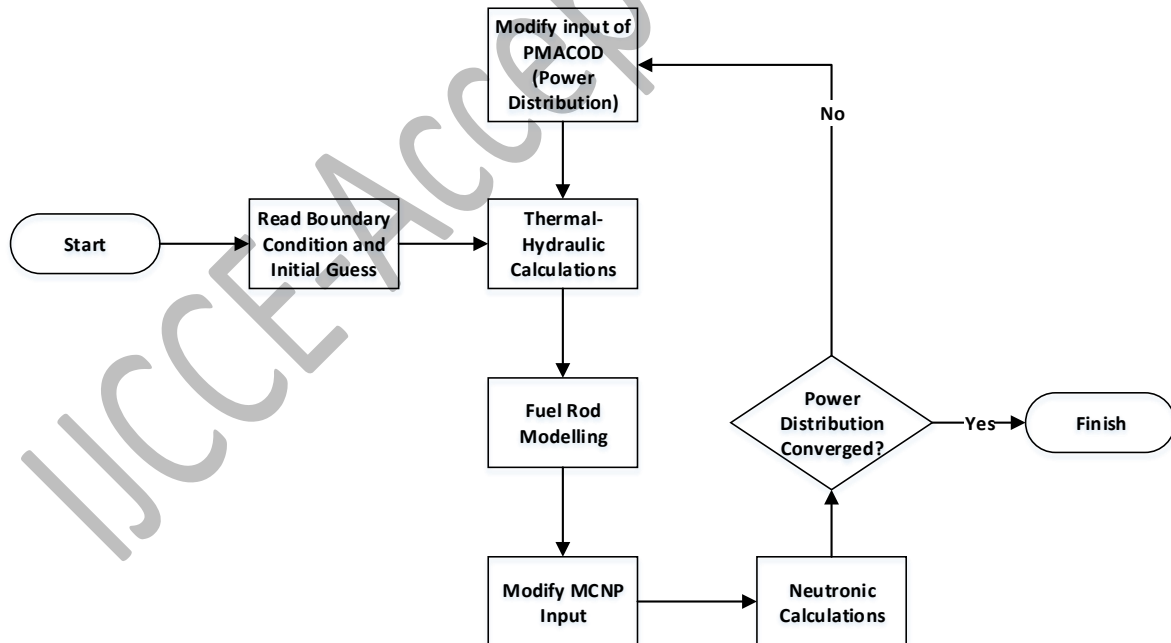


*Fig. 13: Thermo -neutronic calculation flow chart*

## RESULTS AND DISCUSSION

### Benchmark Problem

As it was mentioned in the Introduction, In C. Waata's research [22], the Monte Carlo N-Particle code (MCNP) and the sub-channel code STAFAS (Sub-channel Thermal-Hydraulics Analysis of a Fuel Assembly under

Supercritical Conditions) have been coupled for the design analysis of a fuel assembly with supercritical water as a coolant and moderator. To represent the validation and verification of the thermal-hydraulic approach as well as the neutronic method, a typical SCWR core of those selected by C. Waata [22] is investigated; the reactor core consists of 88 fuel clusters, each of which includes 9 fuel assemblies of BWR-type, which is axially divided into 21 equal control volumes for numerical simulations. Fig. 14 through Fig. 19 represent the variation in thermal-hydraulic properties of the coolant and moderator by applying the axial heat profile, which was reported by C. Waata [22]. Comparison between the archived results and those reported by C. Waata [22] illustrates a maximum error of less than 4.6% (i.e., fuel cladding temperature at z = 0.8 [m]), which in turns indicates the accuracy of the developed model.

In order to benchmark the neutronic calculations, especially the linear heat rate produced by nuclear fission, a coupled thermo-neutronic calculation was performed based on Fig. 13. These calculations were performed by using MCNP computer code with different numbers of initial neutron particles up to 10,000,000 (i.e., 500 cycles with 20,000 initial neutrons); Furthermore, calculations were repeated for two cases: with and without considering 4%-gadolinia ($Gd_2O_3$) rods as burnable absorber material in fuel assemblies [31], see Fig. 20 and Table 4.

Fig. 21 and Fig. 22 illustrate the average linear heat rate generated due to fission in one fuel rod and the radial power peaking factor contour of all fuel assemblies in the reactor, respectively. For the first iteration, the power profile was selected like those reported by C. Waata [22], and the calculation cycle was repeated 17 times until convergence was achieved (see Fig. 21). Comparison between the archived results with those reported by C. Waata [22] illustrates a maximum error of less than 12.3% (i.e., at z = 1.9 [m]), which is mainly due to: a) different calculation conditions (e.g., C. Waata [22] selected 10,000 particles with 700 cycles while the present study was performed for 20,000 particles with 500 cycles), b) using different neutronic libraries, and c) adopting gadolinia burnable material in fuel rods.
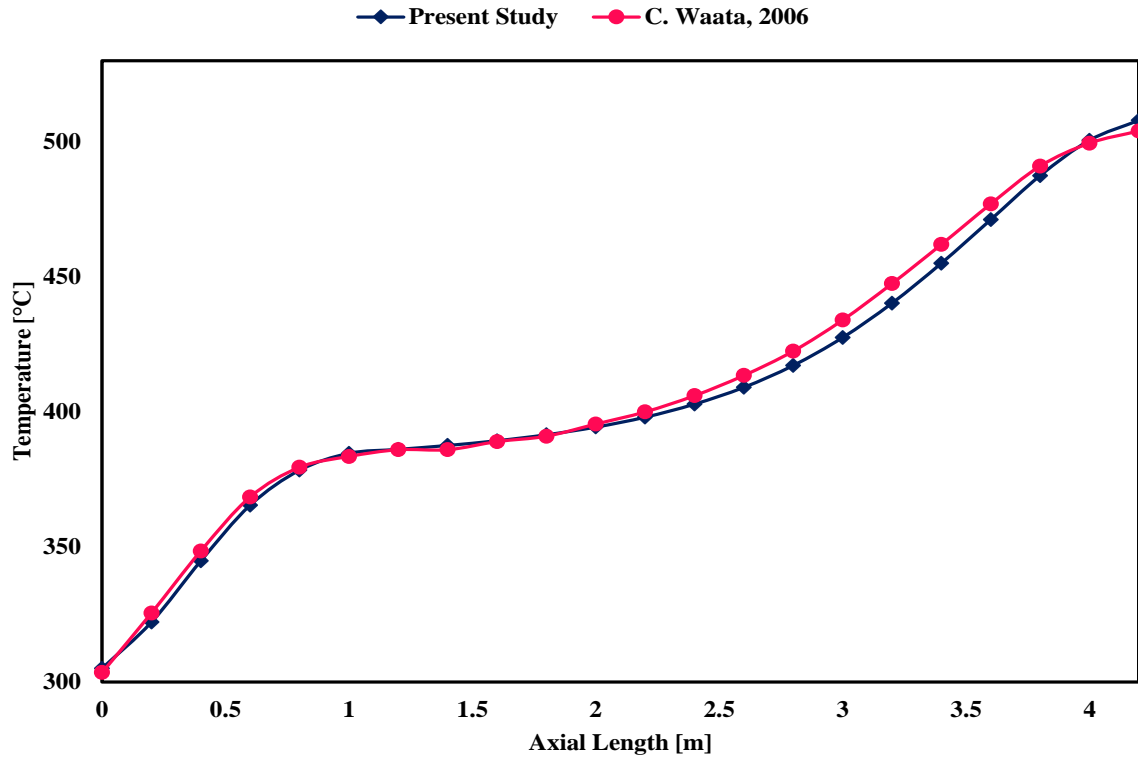
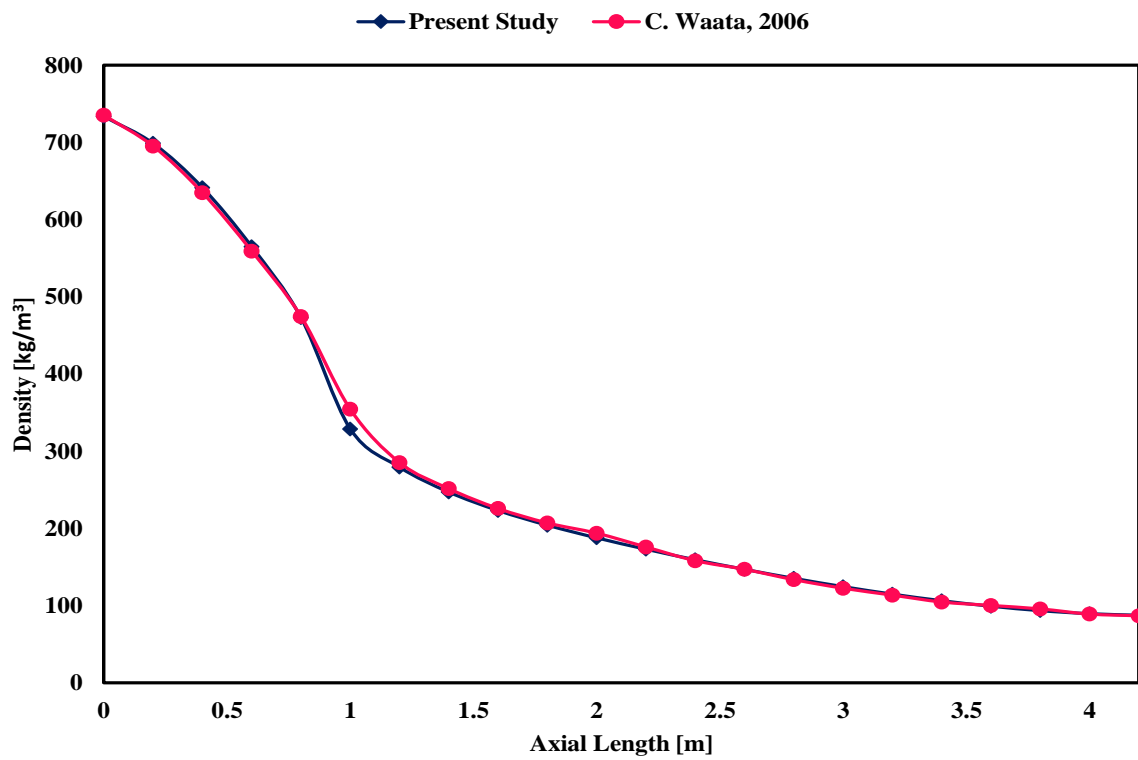*Fig. 14: Variation of average coolant temperature in the reactor core*



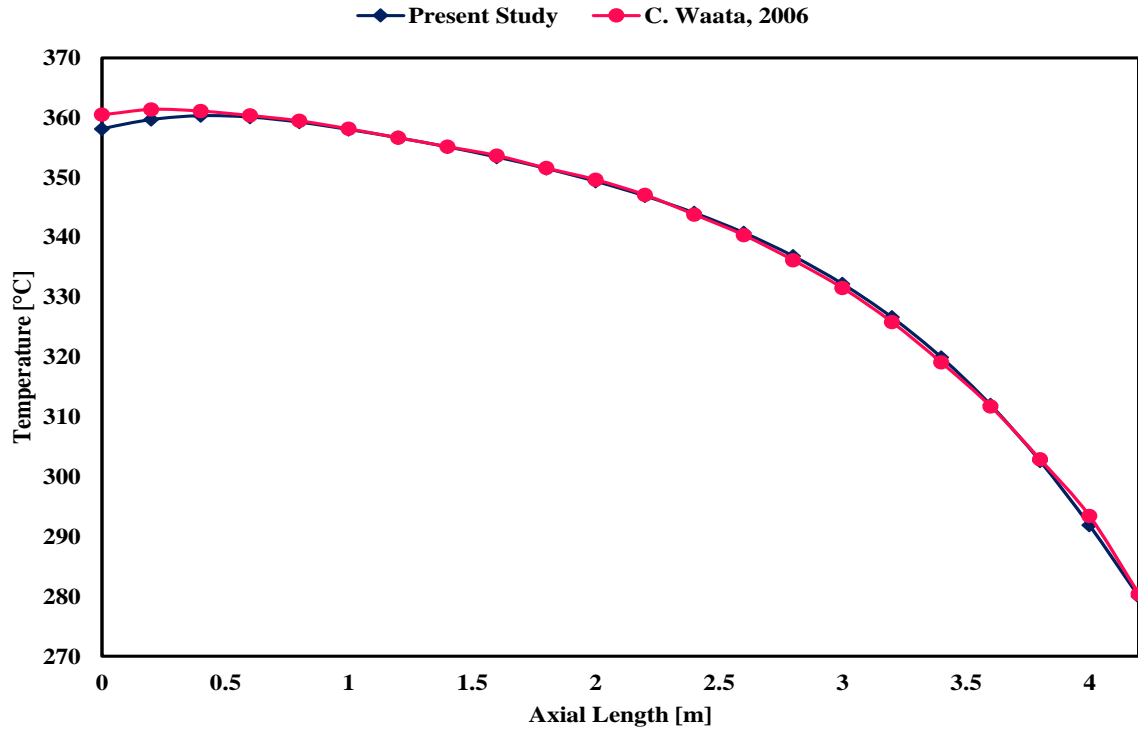*Fig. 15: Variation of average coolant Density in the reactor core*

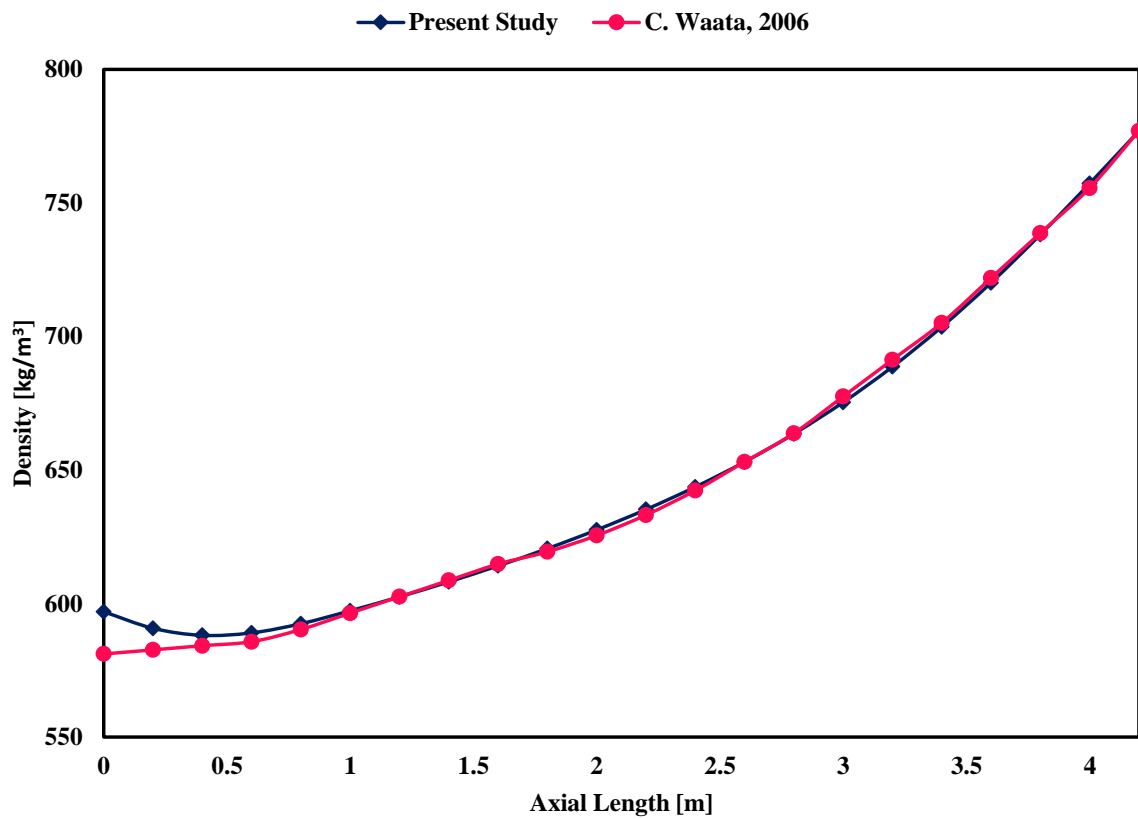*Fig. 16: Variation of average moderator temperature in the reactor core*



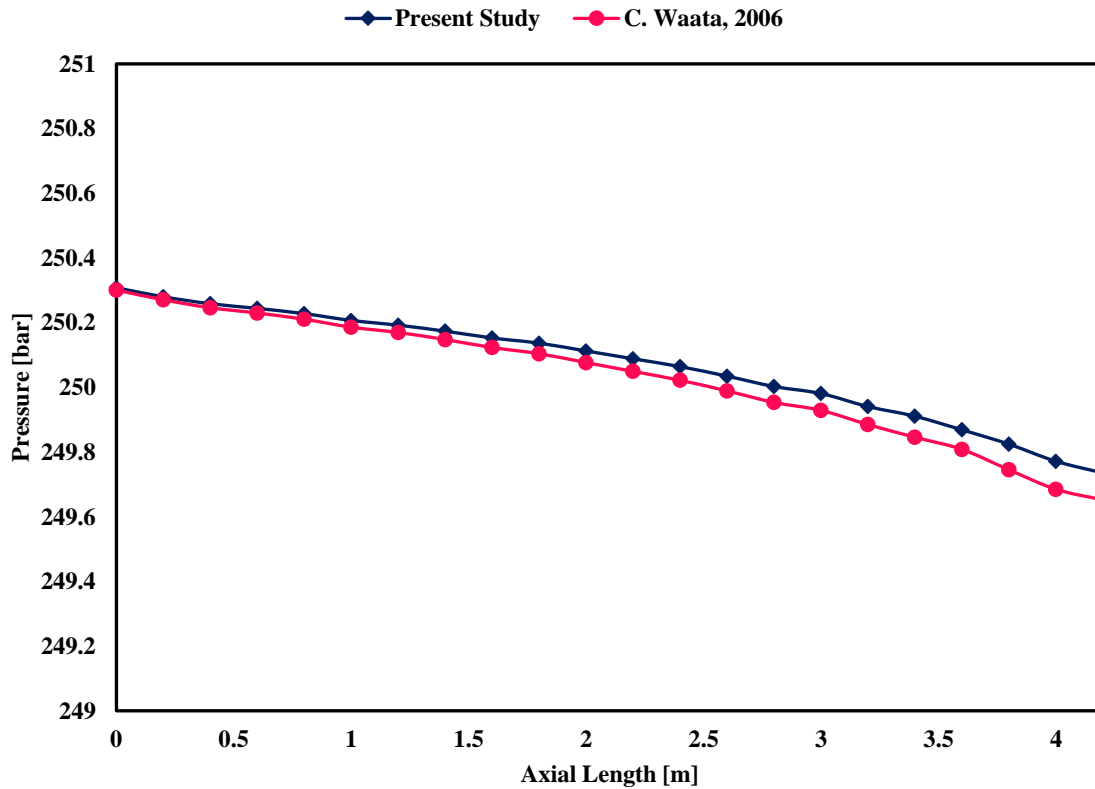*Fig. 17: Variation of average moderator density in reactor core*

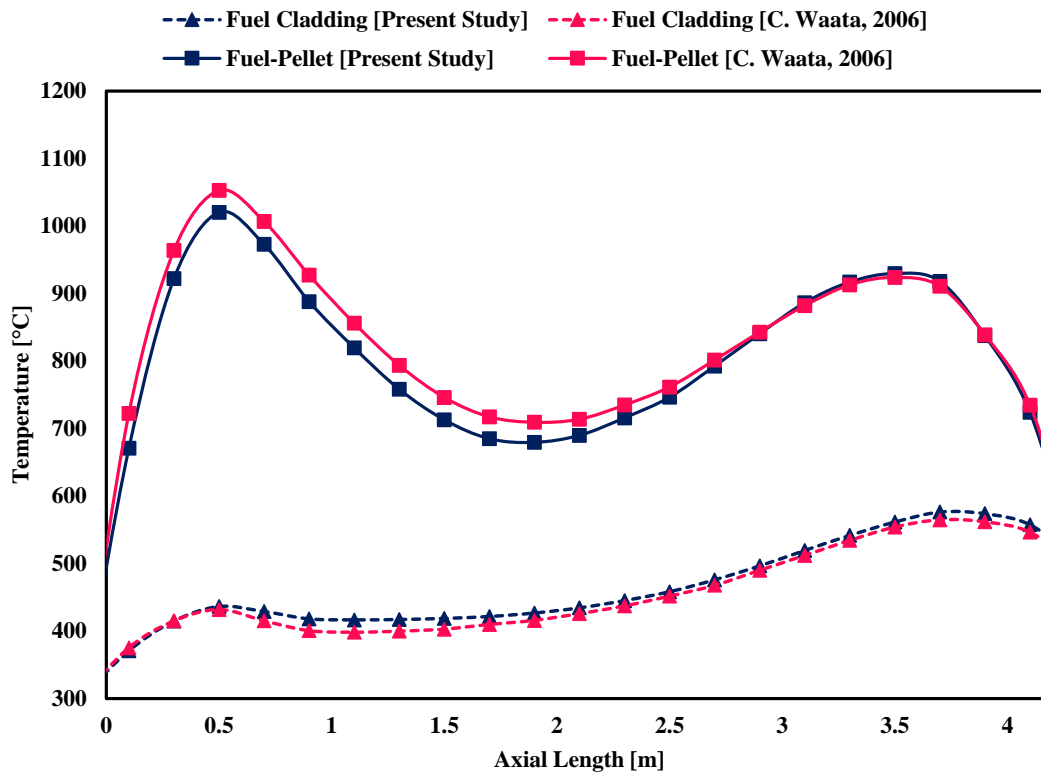*Fig. 18: Variation of average coolant pressure in the reactor core*



*Fig. 19: Variation of average fuel pellet and cladding temperature in the reactor core*

Table 4: Comparison of the effective neutron multiplication factor with previous studies

|  | *Present Study* | *Reference Value* | *Relative error* |
|---|---|---|---|
| $K_{eff}$ *Without Gadolinia* | *1.17765* | *1.17112 [22]* | *0.55 %* |
| $K_{inf}$ *With Gadolinia* | *1.04171* | *1.0352 [31]* | *6.02 %* |
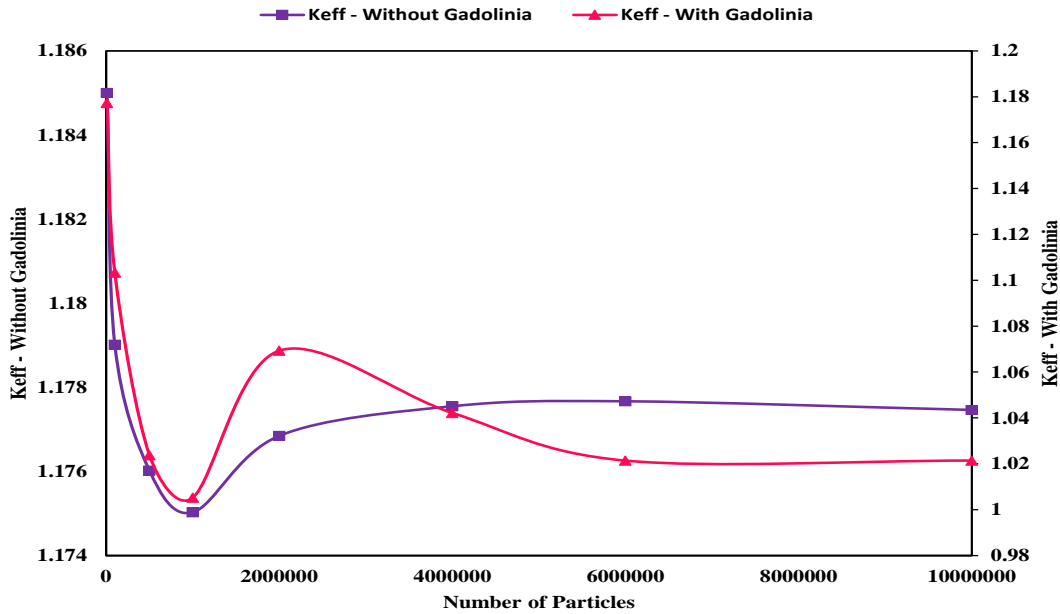


**Fig. 20: Variation of effective neutron multiplication factor vs. number of initial particle**
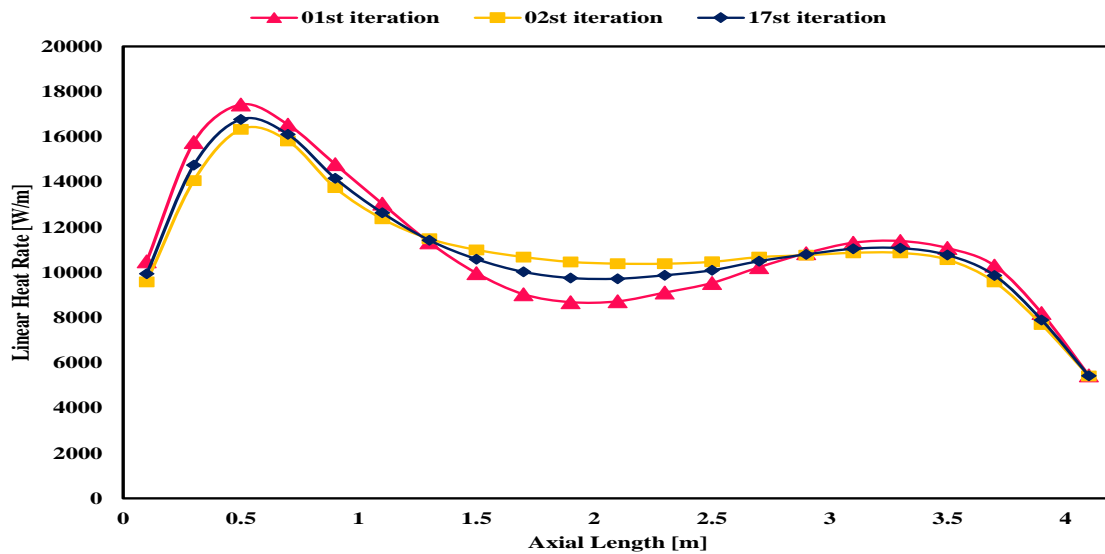


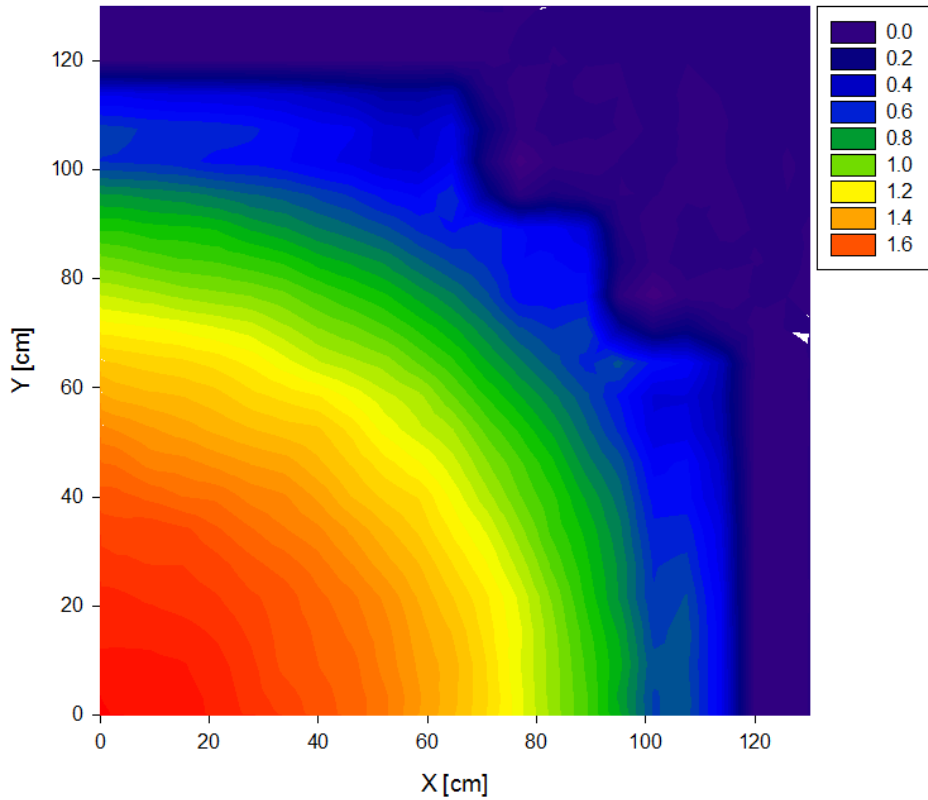**Fig. 21: Variation of the average linear heat rate that is generated in one fuel rod due to nuclear fission**

***Fig. 22: Contour of power peaking factors through the reactor core (by MCNP)***

### Applying nanofluid coolant

The conclusive goal of this study was to investigate the application of nanofluid coolant in a supercritical water reactor. The main characteristics of the selected reactor core and the operating conditions are presented in Table 1. Compared to Al2O3, the average total heat transfer rates are more affected by CuO nanoparticles [32]. Literature review [33, 34] indicates that, among the present nanofluids, Cu-nanoparticle-based nanofluid has the highest thermal efficiency, but the most applicable nanofluid from the neutronic point of view is $Al_2O_3$ nanofluid due to its relatively low neutron absorption cross-section; also, it can be concluded that the reduction in the effective multiplication factor is much milder with alumina nanoparticles. Unlike other nanoparticles, by using alumina, the reactor can remain in the critical state, and the power spectrum is more desirable; hence, in this study, water-based $Al_2O_3$ nanofluid with different mass fractions ($\varphi_M = 0.1\%, 1\%, 5\%, 10\%, 20\% \& 40\%$) were investigated.

Our recent study [21] and literature review showed that many of those who investigated the application of nanofluids in reactors selected the following conditions:

1- Constant mass flow rate before and after applying nanofluid in the reactor, and
2- A constant value for nanoparticles volume fraction through the heated channels.

Here a brief description is provided about the validity of these two assumptions (respectively), and further discussions are left to be described in detail in a separate paper:

1- As one may know, any increase in the mass fraction of nanoparticles in a water-based nanofluid will increase the density of the nanofluid (see Eq.3). Now consider if the coolant mass flow rate ($\dot{m} = \rho A v$) remains constant; when the geometry is not changing, any increase in nanofluid density will simply result in a reduction of velocity. Consequently, this reduction will reduce the convection heat transfer coefficient of the nanofluid (see

Appendix **I**), which is the exact opposite purpose of using nanofluid coolants.

2- Variation on coolant density through the reactor core will change the nanofluid volume fraction, regarding Eq. 2.

Previous mentioned issues indicate that in order to investigate the thermal hydraulic behavior of using nanofluids in nuclear reactors, the inlet mass flow and volume fraction of nanoparticles cannot be assumed to be constant at the same time; instead, a constant inlet velocity for boundary conditions and a constant nanoparticle mass fraction for thermal hydraulic calculations should be adopted. These calculations have been performed theoretically, based on the definition of Nanofluids as stable nanoscale colloidal suspensions containing condensed nanomaterials.

The flow chart presented in Fig. 13 considers the outputs of the benchmark problem as the initial guess for performing calculations is selected for coupled thermo-neutronic simulation. Variation of coolant and moderator temperature through the core is presented in Fig. 23 and Fig. 24. It should be noted that the introduction of $Al_2O_3$ in reactor coolant reduces the specific isobaric heat capacity (see Eq.4 and Fig. 25); if the power and mass flow rate remain constant, based on $Q = \dot{m}.Cp.\Delta T$, any reduction in $Cp$ will result an increase in $\Delta T$, but due to our selected boundary conditions (i.e., constant inlet velocity) based on

Appendix **I**, the outlet temperature remains almost constant, even for $\varphi_M = 40\%$, see Fig. 26.
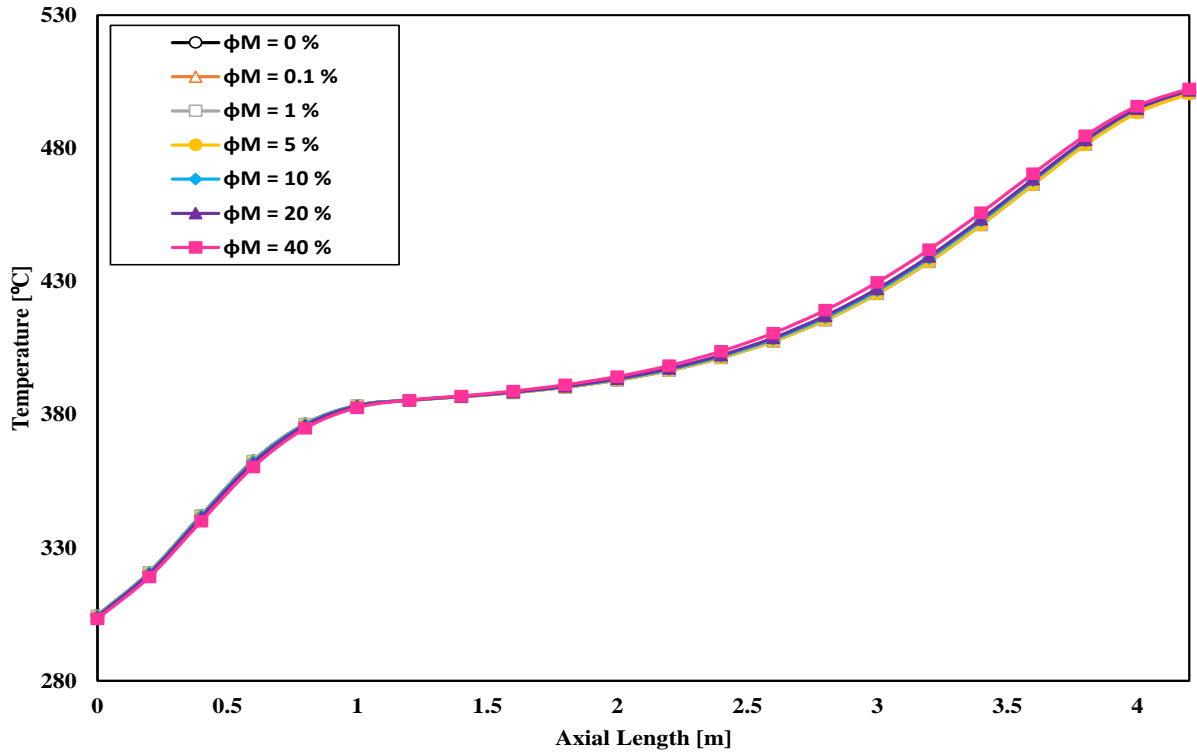
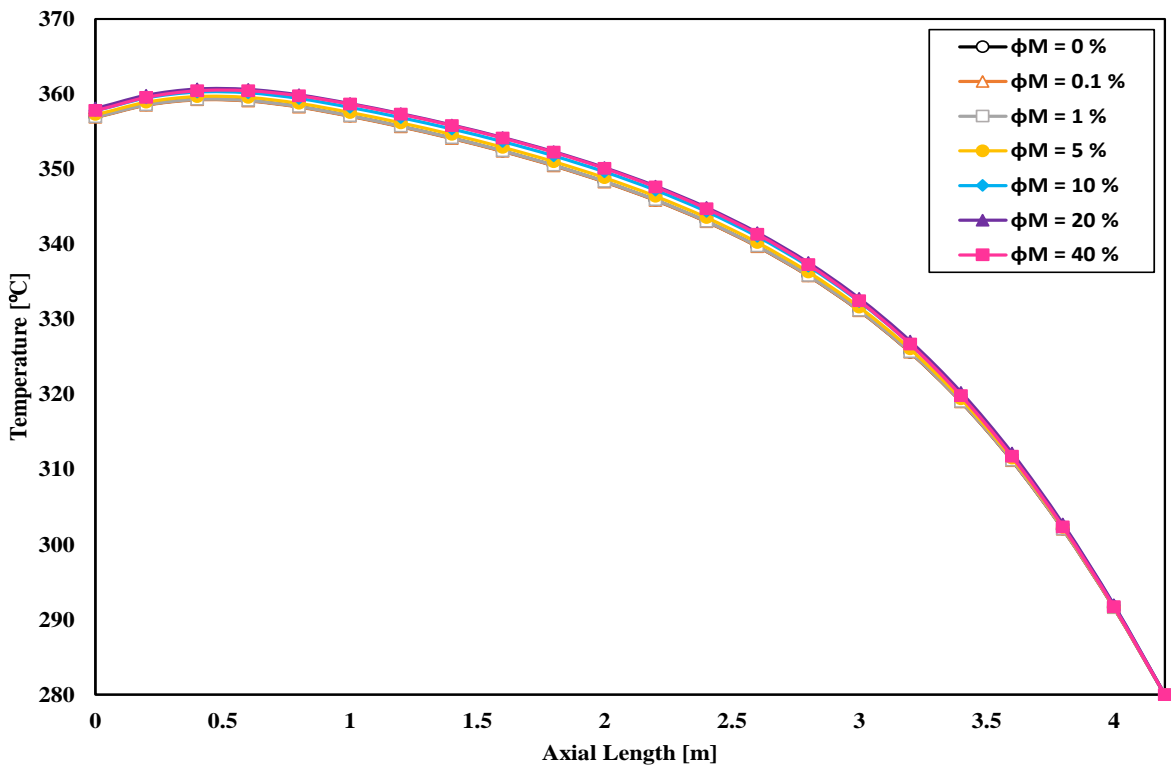*Fig. 23: Variation of average axial Coolant temperature in the reactor core*



*Fig. 24: Variation of average axial moderator temperature in the reactor core*
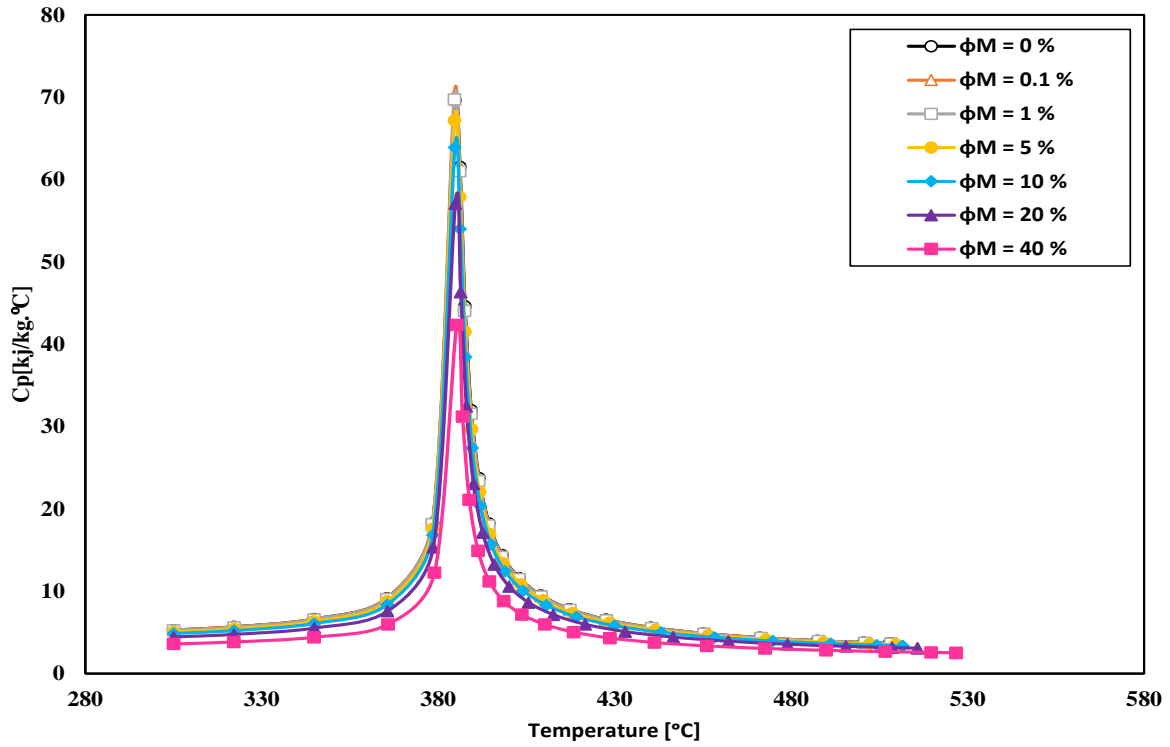
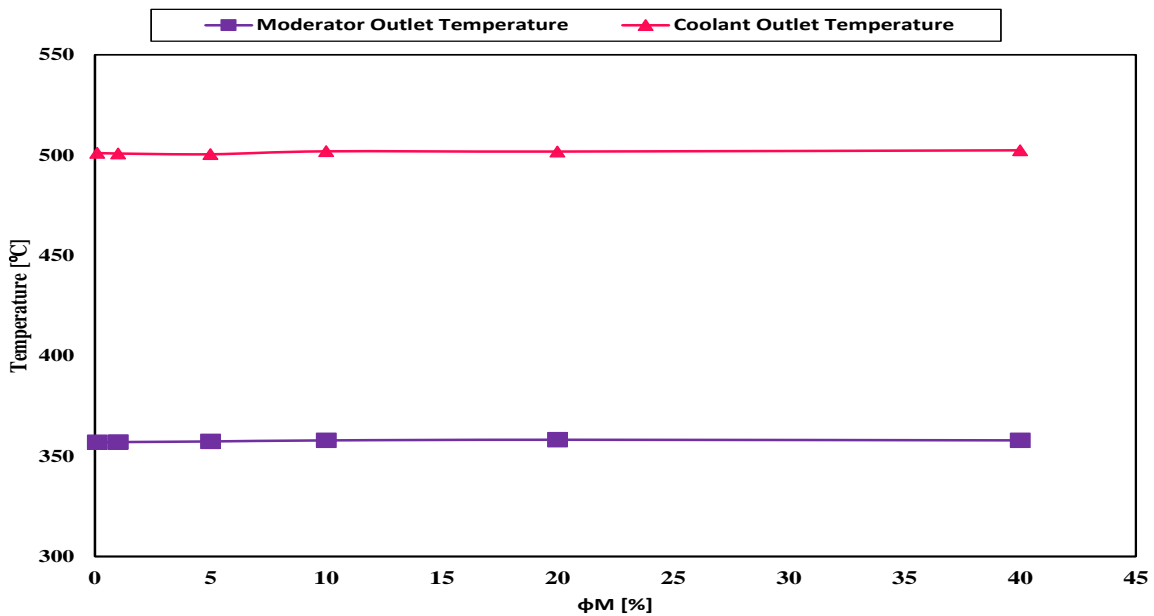*Fig. 25: Specific isobar heat capacity (Cp) of Al2O3 nanofluid with different mass fractions at 25 MPa*



*Fig. 26: Moderator and coolant outlet temperature for different Al2O3 nanofluid mass fractions*

Variation of nanoparticles volume fraction ( $\varphi_V$ ) is depicted in Fig. 27. As mentioned earlier, the achieved results indicate that despite the previous studies of applying nanofluid in reactors [17, 18], the nanoparticles mass fraction

is changed through the reactor core (see Eq.2, 3, 4 and Fig. 28) [21]. According to previous studies, the pressure drop in the core is expected to be higher when the mass fraction of nanoparticles is increased [30]. Combining the nanoparticle and water leads to an increase in the viscosity of the fluid (see Fig. 29). As a consequence, it is expected that the pressure drop through the reactor core will increase subsequently. Reactor coolant pressure drop ( $\Delta P_{Core} = P_{Inlet} - P_{Outlet}$ ) for different nanoparticle mass fractions is depicted in Fig. 29.
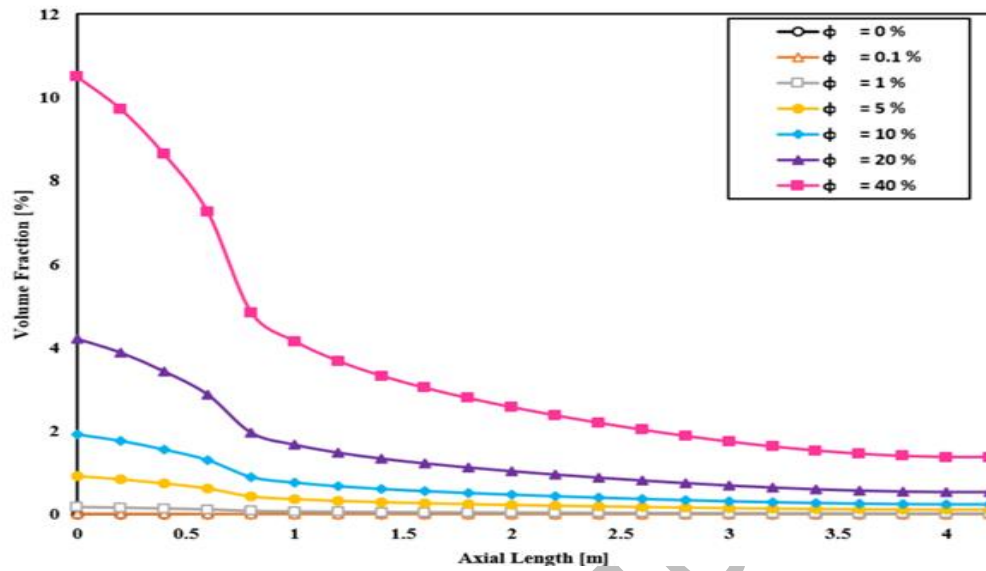


*Fig. 27: Variation of nanoparticles mass fraction in the reactor coolant*
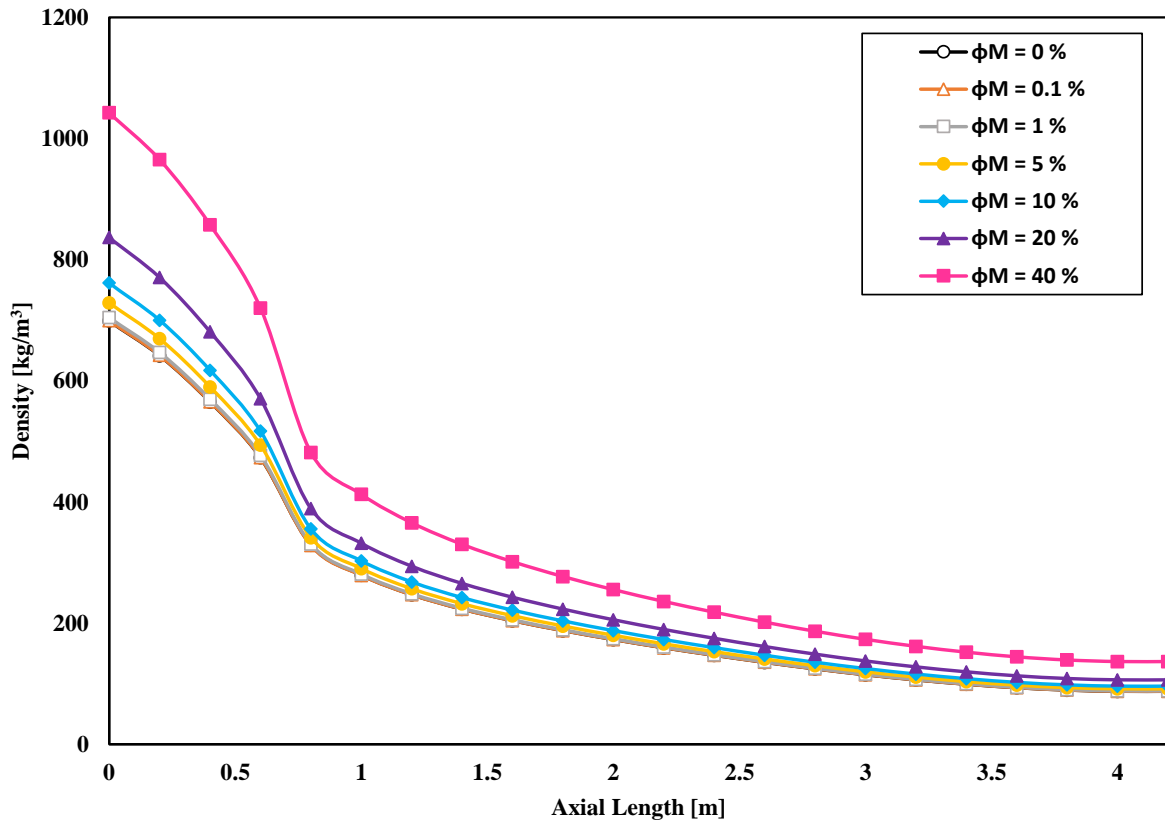
*Fig. 28: Variation of coolant density for different nanoparticles mass fractions*
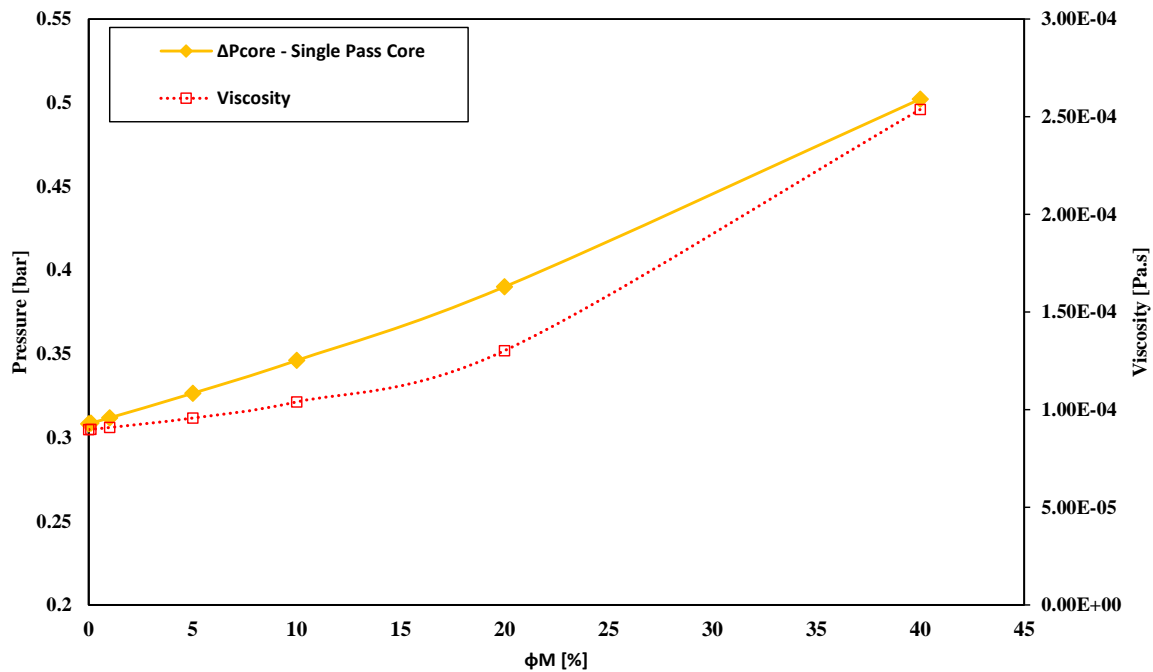


*Fig. 29: Variation of coolant pressure drop and inlet coolant viscosity for different nanoparticles mass fractions*

As mentioned earlier, applying nanofluid coolant in the reactor core will increase the neutron absorption due to the relatively higher neutron cross-section of nanofluid compared with pure water (see Fig. 30). This effect acts just like increasing the concentration of boron solution in reactor coolant to compensate for the excess reactivity of the fuel assemblies; Fig. 30 indicates that, from the $K_{eff}$ point of view, the concentration of nanoparticles can be increased up to $\varphi_M = 11.1305\%$ (where $K_{eff} = 1.000$).

Fig. 31 and Fig. 32 illustrate the radial contour of power peaking factors (from the MCNP code) through the reactor core, as well as the average linear heat rate of one fuel rod for different nanoparticle mass fractions, respectively. Standard deviations of power peaking factors for different nanoparticle mass concentrations are depicted in Fig. 33; this figure shows that, in general, an increase in the nanoparticle mass fraction in the reactor core would reduce the standard deviation of the PPFs between the fuel assemblies, which means the radial distribution of power peaking factors has been flattened.
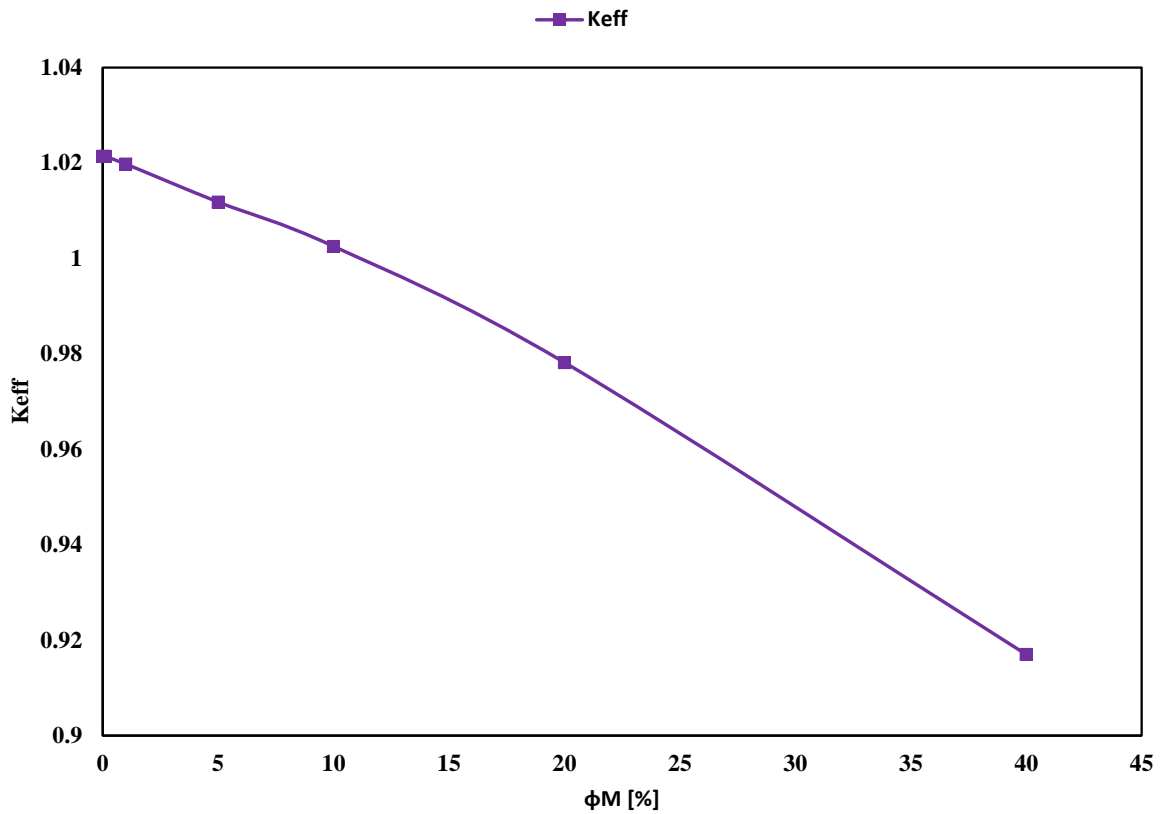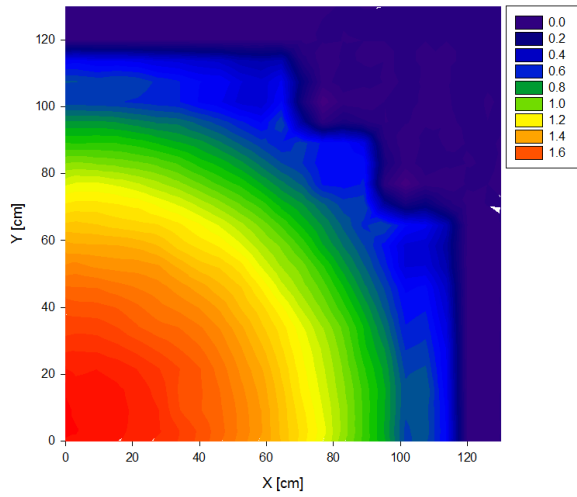


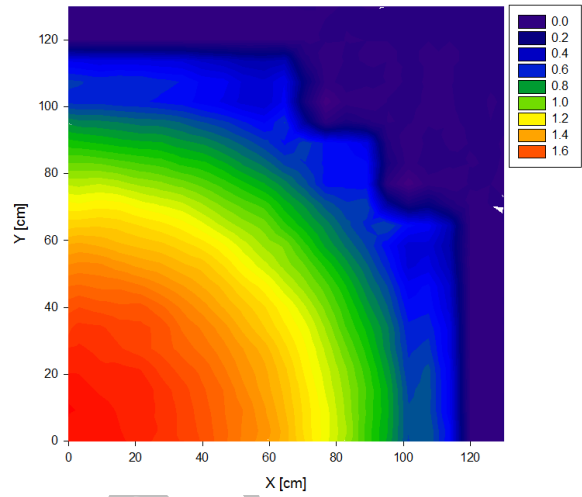***Fig. 30: Effective neutron multiplication factor ($K_{eff}$) of the reactor for different nanoparticle mass fractions***
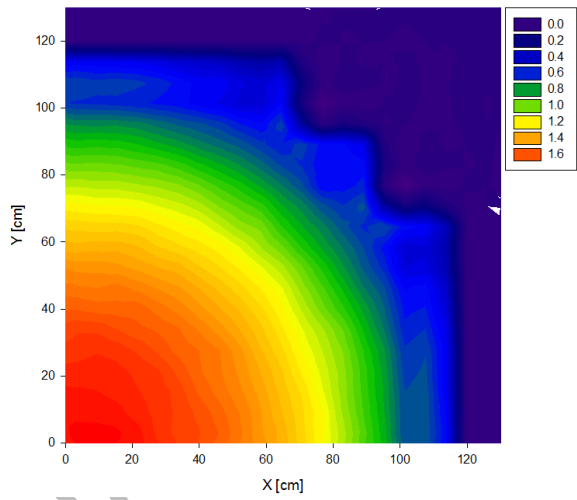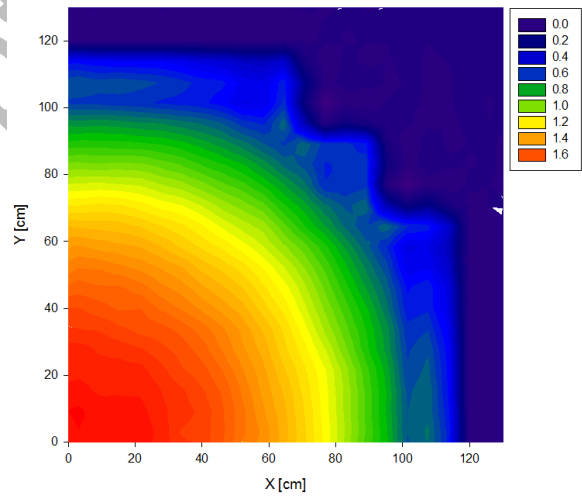
$$\varphi_M = 0.1\%$$



$$\varphi_M = 1\%$$

$$\varphi_M = 5\%$$



$$\varphi_M = 10\%$$

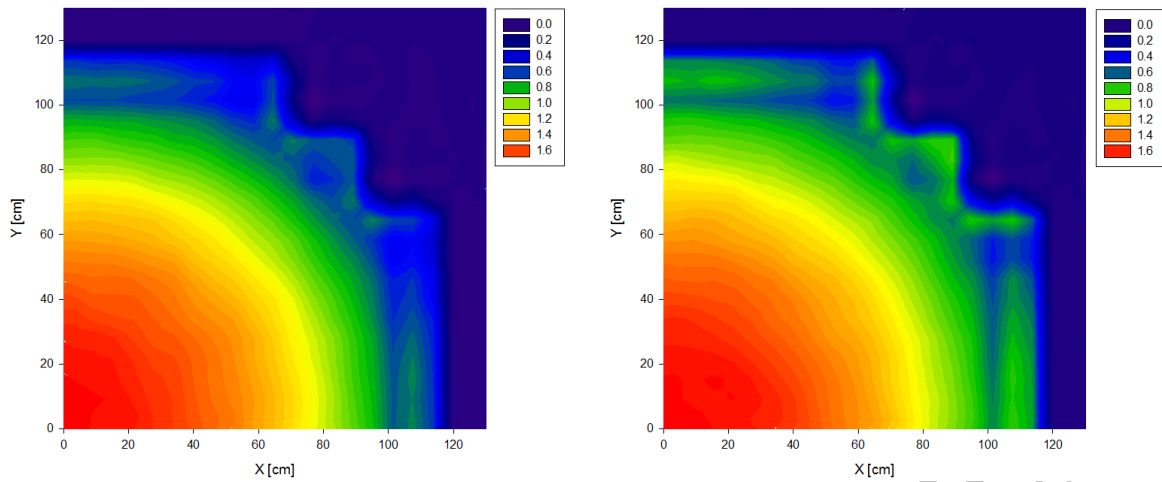$$\varphi_M = 20\%$$

$$\varphi_M = 40\%$$

*Fig. 31: Contour of power peaking factors through the reactor core for different nanoparticle mass fractions*
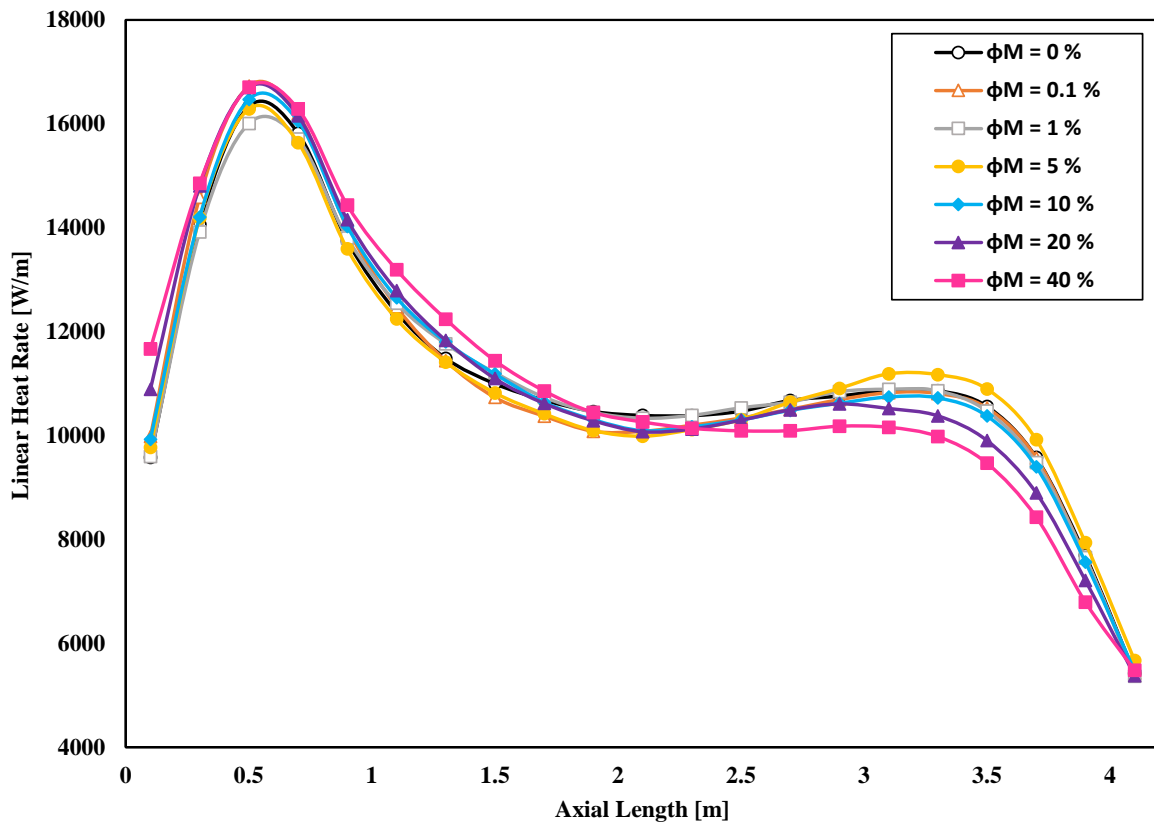


*Fig. 32: Average linear heat rate of one fuel rod for different nanoparticle mass fractions*
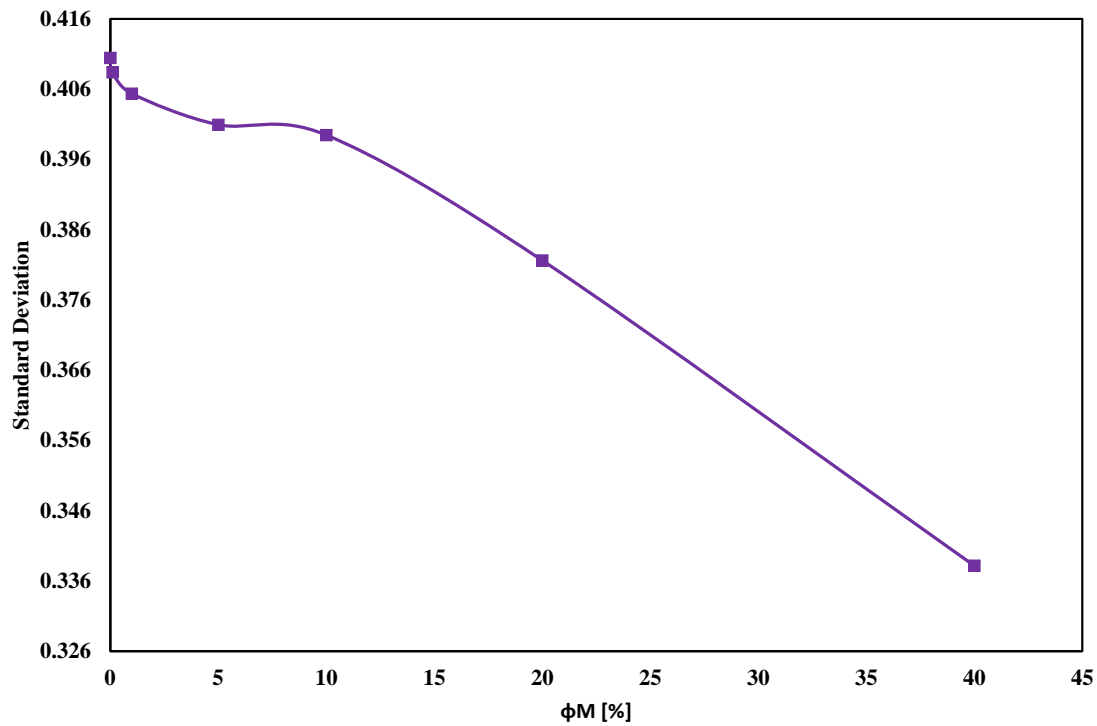
***Fig. 33: Standard deviation of radial core power peaking factors for different nanoparticle mass fractions***

As mentioned earlier, the application of nanofluids is being studied mainly to investigate the improvement of the heat transfer coefficient (HTC) of the coolants. Fig. 34 illustrates the HTC of the coolant in this study. precipitate changes of the fluid properties, including density ($\rho$), specific isobaric heat capacity ($C_P$), viscosity ($\mu$) and thermal conductivity ($K_e$) near the pseudo-critical temperature (PCT), i.e., Axial length~1.5 m, cause an intangible effect on HTC, and the addition of nanoparticles reduces the HTC before PCT, while amplifying the nanoparticles mass fraction increases the HTC after PCT (where the maximum coolant and clad temperature take place at Axial length ~3.8 m, Fig. 35). Fig. 36 shows the HTC enhancement of the coolant at the hottest fuel cladding point per different nanoparticle mass fraction. As one can clearly see, applying waterbased $Al_2O_3$ nanofluid with $\varphi_M = 11.1305\%$ can increase the HTC of the hot channel up to $2\%$ which in turns would reduce the cladding temperature (see Table 5 and Fig. 35).

Table 5: fuel cladding temperature and HTC for different nanoparticles mass fractions at axial length ~3.8 m

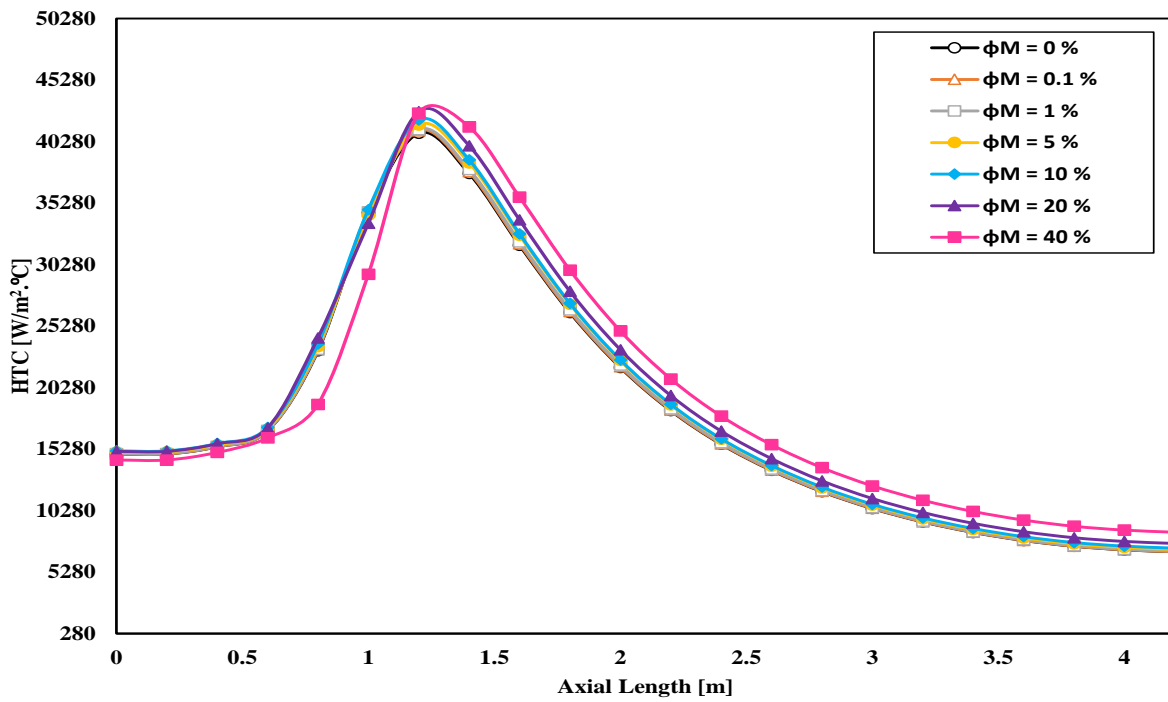| *different nanoparticles mass fractions* | $\varphi_M = 0$ % | $\varphi_M = 0.1$ % | $\varphi_M = 1$ % | $\varphi_M = 5$ % | $\varphi_M = 10$ % | $\varphi_M = 20$ % | $\varphi_M = 40$ % |
|---|---|---|---|---|---|---|---|
| *maximum fuel cladding temperature [•C]* | 558.0409 | 557.696 | 556.6308 | 553.6102 | 553.7277 | 547.1049 | 533.4234 |
| *HTC [W/(m²·•C)]* | 7373.13 | 7382.24 | 7422.13 | 7568.84 | 7678.02 | 8068.52 | 8999.23 |

*Fig. 34: Coolant heat transfer coefficient for different nanoparticles mass fractions*
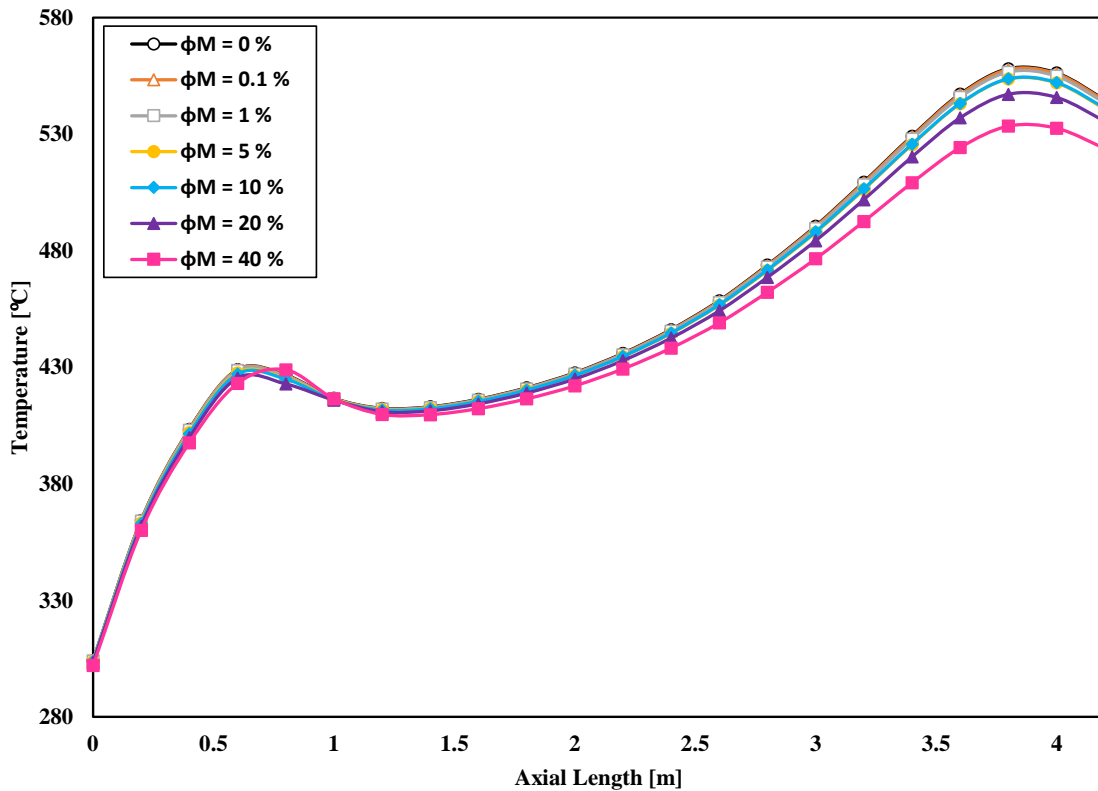


**Fig. 35: Fuel cladding temperature for different nanoparticles mass fractions**
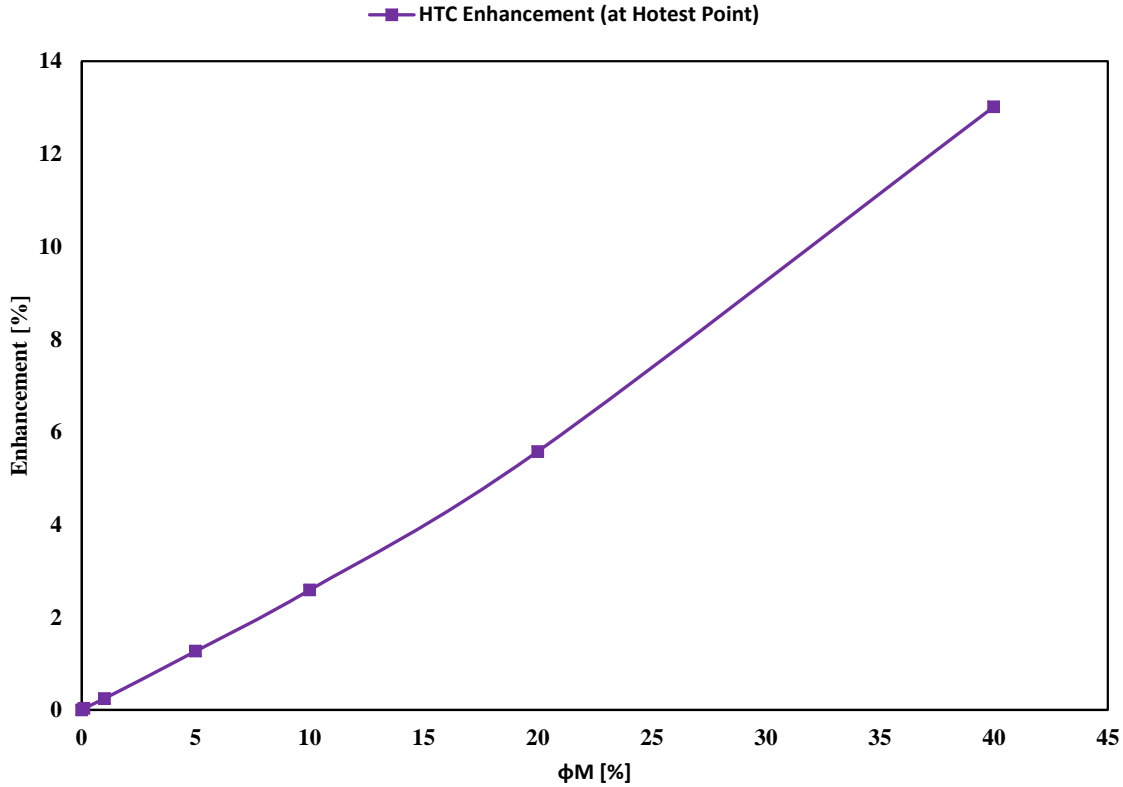
**Fig. 36: Coolant heat transfer coefficient enhancement for different nanoparticles mass fractions at the hottest fuel cladding point**

**CONCLUSION**

One of the main goals of the developments in generation IV nuclear reactors, especially supercritical water reactors, is to improve the thermal efficiency and reduce the construction expenses of the systems. As one knows, in a supercritical water reactor, the coolant does not boil, and therefore the coolant can be heated up as much as the cladding material could resist [13]. Based on Newton's law of cooling, one way to reduce the cladding temperature is to improve the convection heat transfer coefficient of the coolant. Application of nanofluid coolant technology was selected in this study to investigate the possibility of adopting water-based $Al_2O_3$ nanofluid as a coolant in a typical SCWR. In this manner, a coupled thermo-neutronic simulation was performed. The achieved results indicate that:

1- Application of water-based $Al_2O_3$ nanofluid with concentrations of up to $\varphi_M = 11.1305\%$ is possible. as previously mentioned, from the point of view of neutronics, the concentration of nanoparticles can be increased up to the point where the reactor can remain in the critical state (Keff = 1.000).

2- The convection heat transfer coefficient of the coolant can be enhanced up to 2% for nanoparticle mass fraction of $\varphi_M = 11.1305\%$. The maximum temperature of the cladding is the margin of safety, so we calculate the axial length of this crucial point for the selected mass fraction in Fig. 35. The HTC is compared at this axial length of 3.8 m (Fig. 34), and it is evident that the HTC has increased approximately from 7373 W/(m²·°C) for pure water to 7677 W/(m²·°C) for selected nanofluid.

3- The cladding temperature, which is the state of the art of this study, can be reduced 24.6 ° C.

4- By applying water-based $Al_2O_3$ nanofluid as a coolant, the standard deviation of core power peaking factors can be reduced; in other words, the distribution of the power in the reactor core will be more flattened.

An online coupling thermo-neutronic simulation could be used to analyze the abnormal transient operating procedures of nuclear power plants in the future. In order to evaluate their performance, various types and concentrations of nanofluids are suggested for use as coolants in SCWR reactors with diverse design characteristics.

**NOMENCLATURE**

| | | |
|---|---|---|
| $A$ | *Area* ( $m^2$ ) | |
| $g$ | *Acceleration of gravity* ( $m/s^2$ ) | |
| $k_e$ | *Thermal Conductivity* ( $W/m.°C$ ) | |
| $P$ | *Pressure* ( $Pa$ ) | |
| $q$ | *Heat* ( $W$ ) | |
| $q''$ | *Heat flux* ( $W/m^2$ ) | |
| $q'''$ | *Volumetric Heat* ( $W/m^3$ ) | |
| $R$ | *Distributed resistant* ( $Pa/m$ ) | |
| $t$ | *Time* ( $s$ ) | |
| $T$ | *Temperature* ( $°C$ ) | |
| $U$ | *Internal energy* ( $j/kg$ ) | |
| $v$ | *Velocity* ( $m/s$ ) | |
| $V$ | *Volume* ( $m^3$ ) | |
| $\rho$ | *Density* ( $kg/m^3$ ) | |
| $\phi$ | *Dissipation function* ( $W/m^3$ ) | |
| $\varphi_M$ | *Nanoparticle mass fraction* | |
| $\varphi_V$ | *Nanoparticle volume fraction* | |
| $\overline{\overline{\tau}}$ | *Friction Tensor* ( $Pa.m/s$ ) | |
| $\gamma$ | *Porosity* | |

*Subscripts*

| | | |
|---|---|---|
| $A$ | *Surface* | |
| $f$ | *Fluid* | |
| $fs$ | *Total fluid-solid interface* | |

| $T$ | *Total* |
| $V$ | *Volumetric* |
| $x$ | *Direction in Cartesian coordinate system* |
| $y$ | *Direction in Cartesian coordinate system* |
| $z$ | *Axial direction in Cartesian coordinate system* |

**Symbols & Operators**

| $\langle \ \rangle$ | *Volume averaging operator* |
| $\{ \ \}$ | *Surface averaging operator* |

**Abbreviations**

| WWER-1000 | *water water energy reactor - with 1000 MW electrical power* |
| SCWR | *Supercritical Water-Cooled Reactors* |
| HTC | *heat transfer coefficient* |
| PCT | *pseudo-critical temperature* |

## APPENDIX I

Consider a typical hexagonal fuel assembly of a WWER-1000, see Fig. 37. The total area of this assembly is about 0.0472 m$^2$ in which the reactor coolant can flow in an area of about 0.0257 m$^2$ between the fuel rods (Equivalent diameter: $D_e$= 0.0109 m, $D_h$= 0.01159 m). Consider the nominal pressure, temperature and velocity of the coolant at the fuel assembly inlet to be 157 [bar], 291 [° C] and 5.6 [m/s] (inlet mass flow rate = 107.169 [kg/s]), respectively [23]. Thermodynamic and thermal-hydraulic properties of the coolant are summarized in Table 6.
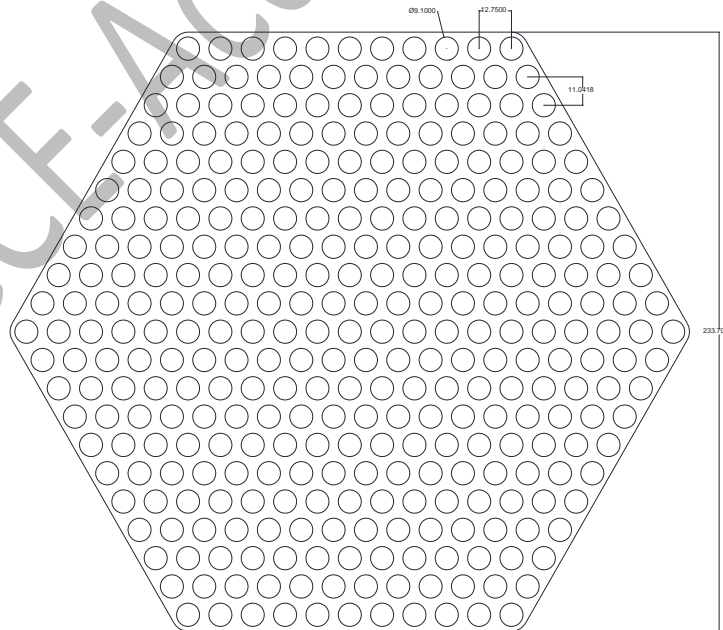


***Fig. 37: Illustration of the WWER-1000 fuel assembly cross-section (dimensions are in mm)***

Table 6: Thermodynamic properties of the coolant [22]

| Property | Value |
|---|---|
| Pressure | 157 [bar] |
| Temperature | 291 [°C] |
| Axial Velocity | 5.6 [m/s] |
| Density | 744.64 [kg/m³] |
| Viscosity | 9.21E-5 [Pa. s] |
| Specific isobar heat capacity | 5.256 [kJ/kg. °K] |
| Thermal conductivity | 0.579 [W/m. °K] |
| Re | 4.93E+5 |
| Pr | 0.83606 |
| Nu (Dittos-Bolter Equation) | 767 |
| Convection heat transfer coefficient | 3.83E+4[W/m². °K] |

For the **same coolant mass flow rate (inlet mass flow rate = 107.169 [kg/s])**, introduction of $Al_2O_3$ nanoparticles with a concentration of $\varphi_V = 1\%$ changes the coolant properties; see Table 7. Comparison between Table 6 and 7 indicates that, despite the previous reports [18, 19], with constant mass-flow rate assumption, the introduction of nanofluid to a WWER-1000 reduces the convection heat transfer coefficient. According to the results [35], the reduction in thermal performance is observed at higher volume fractions than at low concentrations. (Although [36], the rate of heat transfer increases when nanoparticles are added to the base flux).

Table 7: Thermodynamic properties of nanofluid coolant

| Property | Value |
|---|---|
| Pressure | 157 [bar] |
| Temperature | 291 [°C] |
| Axial Velocity | 5.367 [m/s] |
| Density (Eq.3) | 776.89 [kg/m³] |
| Viscosity[18] | 9.24E-5 [Pa. s] |
| Specific isobar heat capacity (Eq.4) | 5.026 [kJ/kg. °K] |
| Thermal conductivity (Eq.6) | 0.595 [W/m. °K] |
| Re | 4.91E+5 |
| Pr | 0.781 |
| Nu (Dittos-Bolter Equation) | 744 |
| Convection heat transfer coefficient | 3.82E+04[W/m². °K] |

**REFERENCES**

[1] Schulenberg T., Starflinger J., "HIGH PERFORMANCE LIGHT WATER REACTOR (Design and Analyses)", KIT Scientific Publishing, (2012).

[2] OKA Y., KOSHIZUKA S., YAMASAKI T., Direct Cycle Light Water Reactor Operating at Supercritical Pressure, *Journal of Nuclear Science and Technology*, **29**(6): 585-588 (1992).

[3] Okano Y., Koshizuka S., Oka Y., Design of water rod cores of a direct cycle supercritical-pressure light water reactor, *Annals of Nuclear Energy,* **21**(10): 601-611 (1994).

[4] Dobashi K., Oka Y., Koshizuka S., Core and plant design of the power reactor cooled and moderated by supercritical light water with single tube water rods, *Annals of Nuclear Energy*, **24**(16):1281-1300 (1997).

[5] Hofmeister J., Waata C., Starflinger J., Schulenberg T., Laurien E., Fuel assembly design study for a reactor with supercritical water, *Nuclear Engineering and Design,* **237**(14):1513-1521 (2007).

[6] Schulenberg T., Starflinger J., Core design concepts for High Performance Light Water Reactors, *Nuclear Engineering and Technology,* **39**(4):249-256 (2007).

[7] Schulenberg T., Starflinger J., Heinecke J., Three pass core design proposal for a high performance light water reactor, *Progress in Nuclear Energy*, **50**(2):526-531 (2008).

[8] Fischer K., Schulenberg T. Laurien E., Design of a supercritical water-cooled reactor with a three-pass core arrangement, *Nuclear Engineering and Design*, **239**(4):800-812 (2009).

[9] Herbell H., Himmel S., Schulenberg T., Mechanical Analysis of an Innovative Assembly Box with Honeycomb Structures Designed for a High Performance Light Water Reactor, *Proceedings of the International Youth Nuclear Congress,* **132**:1-8 (2008).

[10] Bitterman D., Squarer D., Schulenberg T., Oka Y., Dumaz P., Kyrki-Rajamäki R., Aksan N., Maraczy C., Souyri A., Potential plant characteristics of a high performance light water reactor (HPLWR), *International Congress on Advances in Nuclear Power Plants - Proceedings of ICAPP* (2003).

[11] Brandauer M., Schlagenhaufer M., Schulenberg T., Steam cycle optimization for the HPLWR, (2009).

[12] Fischer K., "Design of a Supercritical Water - Cooled Reactor – Pressure Vessel and Internals," (2008).

[13] Zhang L., Bao Y., Tang R., Selection and corrosion evaluation tests of candidate SCWR fuel cladding materials, *Nuclear Engineering and Design,* **249**: 180-187 (2012).

[14] Buongiorno J., Hu L., two-phase heat transfer in water-based nanofluids for nuclear applications, *Nuclear Engineering Education Research (NEER) Program*, 1-347 (2009).

[15] Salehi D., Jahanfarnia G., Zarifi E., Thermal-hydraulic analysis of Al2O3 nanofluid as a coolant in Canadian supercritical water reactor by porous media approach, *Nuclear Engineering and Design*, **368**(5) :110825 (2020).

[16] Choi S., Eastman J., Enhancing thermal conductivity of fluids with nanoparticles, *International mechanical engineering congress and exhibition,* 1-8 (1995).

[17] Saidur R., Leongb K., Mohammad H., A review on applications and challenges of nanofluids, *Renewable and Sustainable Energy Reviews,* **15**(3): 1646–1668 (2011).

[18] Zarifi E., Jahanfarnia G., Veysi F., Thermal-hydraulic modeling of nanofluids as the coolant in VVER-1000 reactor core by the porous media approach, *Annals of Nuclear Energy,* **51**: 203–212 (2013).

[19] Safarzadeh O., Shirani A., Minuchehr A., Saadatian-derakhshandeh F., Coupled neutronic/thermo-hydraulic analysis of water/Al2O3 nanofluids in a VVER-1000 reactor, *Annals of Nuclear Energy,* **65**: 72-77, (2014).

[20] Nourollahi R., Esteki M. H., Jahanfarnia G., Neutronic analysis of a VVER-1000 reactor with nanofluid as coolant through zeroth order average current nodal expansion method, *Progress in Nuclear Energy*, **116**: 46-61 (2019).

[21] Rahimi M., Jahanfarnia G., Vosoughi N., Thermal–hydraulic analysis of nanofluids as the coolant in supercritical water reactors, *The Journal of Supercritical Fluids,* **128** : 47-56 (2017).

[22] Waata C. L., Coupled neutronics, thermal–hydraulics analysis of a high performance light-water reactor fuel assembly, (2006).

[23] Rahimi M., Jahanfarnia G., Thermal-hydraulic core analysis of the VVER-1000 reactor using a porous media approach, *Journal of Fluids and Structures,* **51**: 85–96 (2014).

[24] Rahimi M., Jahanfarnia G., Thermo-hydraulic analysis of the supercritical water-cooled reactor core by porous media approach, *The Journal of Supercritical Fluids,* **110**: 275–282 (2016).

[25] Hagrman D., Reymann G., "MATPRO-Version 11: a handbook of materials properties for use in the analysis of light water reactor fuel rod behavior", Idaho National Engineering Lab., Idaho Falls (USA) (1979).

[26] Luscher W., Geelhood K., "Material Property Correlations: Comparisons between FRAPCON-3.4, FRAPTRAN 1.4, and MATPRO", Pacific Northwest National Laboratory, Richland (2010).

[27] Todreas N. E., Kazimi M. S., "Nuclear systems - THERMAL HYDRAULIC FUNDAMENTALS", 1 (2011).

[28] Hosseini S. A., Athari Allaf M., Implementation and benchmarking of ENDFVII based library for PBM reactor analysis with MCNP4c, *Progress in Nuclear Energy*, **60**: 27-30 (2012).

[29] Conti A., "Impact of neutron thermal scattering laws on the burn-up analysis of Supercritical LWR's fuel assemblies", Universität Stuttgart, (2011).

[30] Bahrevar M.H., Jahanfarnia G., pazirandeh A., Shayesteh M., Thermal-hydraulic analysis of a novel design super critical water reactor with Al2O3 nanofluid as a coolant, *The Journal of Supercritical Fluids*, **140**: 41-52

[31] Barragán-Martínez A.-M., Martin-del-Campo C., François J.-L., Espinosa-Paredes G., MCNPX and HELIOS-2 comparison for the neutronics calculations of a Supercritical Water Reactor HPLWR, Annals of Nuclear Energy, **51**: 181–188 (2013).

[32] Atashafrooz, M., Influence of radiative heat transfer on the thermal characteristics of nanofluid flow over an inclined step in the presence of an axial magnetic field, *J Therm Anal Calorim*, **139**: 3345–3360 (2020).

[33] Zarifi E., Jahanfarnia G., Veysi F., Neutronic simulation of water-based nanofluids as a coolant in VVER-1000 reactor, Progress in Nuclear Energy, **65**: 32-41(2013).

[34] Mirghaffari R., Jahanfarnia G., Athari Allaf M., Neutronic simulation of a CANDU-6 reactor with heavy water-based nanofluid coolant, Nuclear Technology and Radiation Protection, **32**(4): 320-326 (2017).

[35] Chamkha, A. J., Armaghani, T., Mansour, M. A., Rashad, A. M., Kargarsharifabad, H., MHD Convection of an Al2O3–Cu/Water Hybrid Nanofluid in an Inclined Porous Cavity with Internal Heat Generation/Absorption, *Iranian Journal of Chemistry and Chemical Engineering*, **41**(113), 936-956(2022).

[36] Sajjadi H., Amiri Delouei A., Atashafrooz M., Sheikholeslami M., Double MRT Lattice Boltzmann simulation of 3-D MHD natural convection in a cubic cavity with sinusoidal temperature distribution utilizing nanofluid, *International Journal of Heat and Mass Transfer*, Volume **126**: 489-503(2018)